

# RMNP: Row-Momentum Normalized Preconditioning for Scalable Matrix-Based Optimization

Shenyang Deng<sup>1,\*</sup>, Zhuoli Ouyang<sup>1,\*</sup>, Tianyu Pang<sup>1</sup>, Zihang Liu<sup>2,3</sup>,  
Ruo Chen Jin<sup>1</sup>, Shuhua Yu<sup>4</sup>, Yaoqing Yang<sup>1</sup>

<sup>1</sup>Dartmouth College

<sup>2</sup>International Computer Science Institute

<sup>3</sup>University of California, Berkeley

<sup>4</sup>Meta

<sup>1</sup>{shenyang.deng.gr, zhuoli.ouyang.gr, tianyu.pang.gr, ruochen.jin.gr, yaoqing.yang}@dartmouth.edu

<sup>2,3</sup>zihang.liu@berkeley.edu <sup>4</sup>yu.shuhuaxh@gmail.com

## Abstract

Preconditioned adaptive methods have gained significant attention for training deep neural networks, as they capture rich curvature information of the loss landscape. The central challenge in this field lies in balancing preconditioning effectiveness with computational efficiency of implementing the preconditioner. Among recent advances, MUON stands out by using Newton-Schulz iteration to obtain preconditioned updates without explicitly constructing the preconditioning matrix. Despite its advantages, the efficiency of MUON still leaves room for further improvement. In this paper, we introduce RMNP (Row Momentum Normalized Preconditioning), an optimizer that replaces Newton-Schulz iteration with a simple row-wise  $\ell_2$  normalization operation, motivated by the empirically observed diagonal block structure of the Transformer layerwise Hessian. This substitution reduces the per-iteration computational complexity from  $\mathcal{O}(mn \cdot \min(m, n))$  to  $\mathcal{O}(mn)$  for an  $m \times n$  weight matrix while maintaining comparable optimization performance. Theoretically, we establish convergence guarantees for RMNP in the non-convex setting that match recent results for MUON optimizers, achieving the information-theoretic minimax optimal complexity. Extensive experiments on large language model pretraining show that RMNP delivers competitive optimization performance compared with MUON while substantially reducing preconditioning wall-clock time. Our code is available at [this link](#).

## 1 Introduction

Adaptive algorithms, such as those introduced in Duchi et al. [1], Tieleman and Hinton [2], Kingma and Ba [3], Loshchilov and Hutter [4], have achieved remarkable success in deep learning optimization. These methods employ diagonal preconditioning [1], which scales each parameter independently based on historical gradient information. However, this diagonal structure ignores correlations among parameters, limiting the optimizer’s ability to handle ill-conditioned problems with complex parameter interactions. This creates a fundamental gap between practical diagonal methods and the theoretically optimal full-matrix preconditioning.

Recent work has revisited matrix-based preconditioning to address these limitations. In particular, studies on full Gauss-Newton methods [5] demonstrate that utilizing complete curvature information can lead to qualitatively improved convergence behavior in large language models. However, directly applying updates of the form  $w_t = w_{t-1} - H_t^{-1}d_t$  remains computationally prohibitive: if the preconditioner  $H_t$  is constructed

---

\*Indicates equal contribution.

Algorithm 1: MUON [11]

**Require:**  $\eta_t > 0, \beta \in [0, 1), W_0 \in \mathbb{R}^{m \times n}$ , loss  $f$

- 1:  $V_0 \leftarrow \mathbf{0}_{m \times n}$
- 2: **for**  $t = 1$  to  $T$  **do**
- 3:    $G_t \leftarrow \nabla f(W_t; \xi^t)$
- 4:    $V_t \leftarrow \beta V_{t-1} + (1 - \beta)G_t$
- 5:    $D_t \leftarrow \text{NS}_5(V_t)$ ,  $D_t = (V_t V_t^T)^{-\frac{1}{2}} V_t$
- 6:    $W_{t+1} \leftarrow W_t - \eta_t D_t$
- 7: **end for**

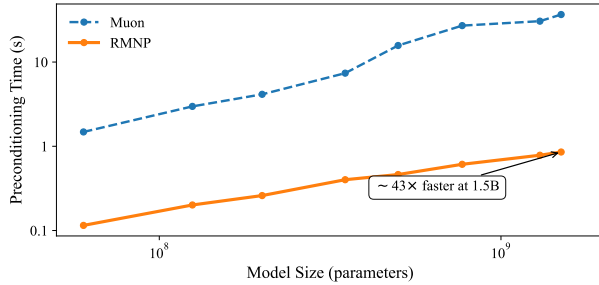


Figure 1: Time overhead comparison. The figure illustrates the wall-clock time for 100 computation steps for preconditioning process of RMNP versus MUON.

Algorithm 2: RMNP

**Require:**  $\eta_t > 0, \beta \in [0, 1), W_0 \in \mathbb{R}^{m \times n}$ , loss  $f$

- 1:  $V_0 \leftarrow \mathbf{0}_{m \times n}$
- 2: **for**  $t = 1$  to  $T$  **do**
- 3:    $G_t \leftarrow \nabla f(W_t; \xi^t)$
- 4:    $V_t \leftarrow \beta V_{t-1} + (1 - \beta)G_t$
- 5:    $D_t \leftarrow \text{RN}(V_t)$ ,  $D_t = \text{diag}((V_t V_t^T)^{-\frac{1}{2}}) V_t$
- 6:    $W_{t+1} \leftarrow W_t - \eta_t D_t$
- 7: **end for**

Work	Smooth	Conv.	Complexity
<i>MUON</i>			
[16]	$L_F$	$\ \nabla f\ _*$	$O(m^2 L \sigma^2 \Delta \epsilon^{-4})$
[17]	$L_*$	$\ \nabla f\ _*$	$O(m L_* \sigma^2 \Delta \epsilon^{-4})$
[16]	$L_*$	$\ \nabla f\ _*$	$O(m L_* \sigma^2 \Delta \epsilon^{-4})$
<i>RMNP</i>			
Thm. 5.5	$L_F$	$\ \nabla f\ _F$	$O(m^2 L_F \sigma^2 \Delta \epsilon^{-4})$
Thm. 5.7	$L_F$	$\ \nabla f\ _{1,2}$	$O(m^2 L_F \sigma^2 \Delta \epsilon^{-4})$
Thm. 5.9	$L_{\infty,2}$	$\ \nabla f\ _{1,2}$	$O(m L_{\infty,2} \sigma^2 \Delta \epsilon^{-4})$

Table 1: Comparison of Convergence Results.  $L_F, L_*$  denotes the corresponding smoothness coefficient and  $\|\nabla f\|_F, \|\nabla f\|_*$  the corresponding convergence criterion.

using the full Hessian, the computational overhead becomes extreme and scales poorly with model size. Consequently, practical optimizer design has focused on structured approximations with first-order information to balance performance with efficiency.

Classic methods such as K-FAC [6], PSGD [7], and SHAMPOO [8] achieve this balance through structured matrix preconditioners that approximate curvature with lower-dimensional factors. SHAMPOO, for example, employs a Kronecker-factored preconditioner:

$$H = L \otimes R \quad (1)$$

where  $L$  and  $R$  are smaller matrices capturing row and column correlations, respectively. This factorization preserves essential curvature information while dramatically reducing computational demands. Subsequent works including K-BFGS [9] and ASGO [10] further refine this approach with sparse or low-rank updates to minimize memory overhead.

More recently, methods such as MUON [11] have introduced an alternative perspective on matrix-based adaptivity (see Algorithm 1). Rather than explicitly forming the full preconditioner  $H^{-1}$ , MUON employs Newton-Schulz iterations to implicitly compute the preconditioned updates  $H_t^{-1} d_t$  through matrix polynomials, enabling matrix-level adaptation without direct inversion. Subsequent refinements further improve the stability and efficiency of this approach [12, 13, 14, 15]. Overall, these methods move beyond element-wise diagonal preconditioning by incorporating structured off-diagonal curvature information, aiming to achieve a **better trade-off between optimization performance and computational cost**. However, despite this conceptual advancement, the reliance on iterative matrix polynomial evaluations in MUON incurs a computational complexity of  $\mathcal{O}(mn \cdot \min(m, n))$  for an  $m \times n$  weight matrix, which can become a dominant bottleneck as model dimensions grow.

In this paper, we show that the computational complexity of MUON can be further reduced without sacrificing its matrix-level adaptivity. Specifically, motivated by recent empirical and theoretical findings on the structure of Transformer Hessians [18, 19], we introduce Row Momentum Normalized Preconditioning

(RMNP, Algorithm 2). RMNP achieves optimization performance comparable to MUON while substantially reducing the preconditioning overhead, with a per-iteration computational complexity of  $\mathcal{O}(mn)$ . We further benchmark the wall-clock time of both optimizers under identical settings, as shown in Figure 1, demonstrating an order-of-magnitude reduction in preconditioning cost.

Mechanistically, RMNP replaces the Newton-Schulz iteration in MUON with a simple row-wise  $\ell_2$  normalization. In Section 3.1, we provide a mathematical interpretation of this operation from a preconditioning perspective, showing that it corresponds to a further structured approximation of K-FAC aligned with the observed block-diagonal dominance of Transformer curvature. We also discuss how RMNP differs from related approaches and provide practical hyperparameter recommendations. Furthermore, we provide non-convex convergence guarantees for RMNP. As summarized in Table 1, our results match the best-known theoretical guarantees for MUON [16, 17]. This complexity result achieves the minimax optimality in non-convex smooth setup [20]. For more related work, please refer to the Appendix 2.

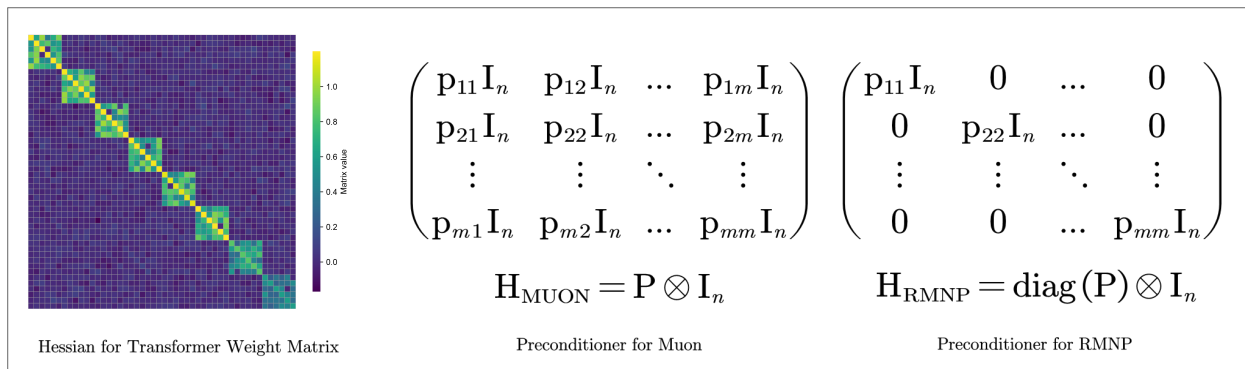


Figure 2: Comparison among Transformer layerwise Hessian, Preconditioner for MUON, and Preconditioner for RMNP. The figure of Transformer layerwise Hessian is conceptual, the real case can be widely found in [18, 19].  $\mathbf{P} = (\mathbf{V}_t \mathbf{V}_t^T)^{\frac{1}{2}}$ ,  $m$  and  $n$  are the number of rows and columns of the weight matrix, respectively. In Section 3.2 we further verified through experiments that the MUON preconditioner has such a certain diagonal dominance property.

Our key contributions are summarized as follows:

- **Structure-Aware Preconditioning with Lower Computational Complexity.** We propose RMNP, a matrix-based adaptive optimizer that replaces Newton-Schulz iterations in MUON with a row-wise  $\ell_2$  normalization operation motivated by the observed block-diagonal dominance of Transformer curvature. This design preserves matrix-level adaptivity while reducing the per-iteration computational complexity from  $\mathcal{O}(mn \cdot \min(m, n))$  to  $\mathcal{O}(mn)$ .
- **Empirical Analysis and Evaluation on Large Language Models.** We empirically validate the diagonal dominance properties of the MUON preconditioner that underlie our design hypothesis. We also conduct comparative experiments across various model architectures spanning multiple scales. Our results demonstrate that RMNP consistently matches or exceeds the final perplexity of MUON while achieving up to an order-of-magnitude reduction in preconditioning wall-clock time.
- **Non-Convex Convergence Guarantees.** We establish convergence analysis for RMNP under the non-convex smooth setting. Our theoretical results provide convergence guarantees that are on par with the current state-of-the-art theory for MUON, ensuring the robustness of our proposed method despite the reduced complexity. We also show that our results achieve minimax optimal complexity.

## 2 Related Work

**Preconditioned Optimization Algorithms** Preconditioned optimization methods aim to reshape the gradient by incorporating curvature information, thereby accelerating convergence in ill-conditioned problems. Early approaches such as ADAGRAD [1] and RMSPROP [2] employ diagonal preconditioning that adapts to the per-coordinate geometry of gradients. While computationally efficient, diagonal preconditioners fail to capture parameter correlations that naturally arise in neural network training. To address this limitation, matrix-based preconditioning methods have been developed. K-FAC [6] approximates the Fisher information matrix using Kronecker-factored structure, exploiting the layer-wise organization of neural networks. PSGD [7, 21] introduces Lie group preconditioners that maintain geometric properties during optimization. SHAMPOO [8] generalizes preconditioning to tensor spaces, maintaining separate preconditioners for each dimension through Kronecker factorization. Recent work has further improved upon SHAMPOO, with SOAP [13] stabilizing it through Adam-style updates, while distributed implementations [22] enable scaling to large models. Extensions such as K-BFGS [9] and ASGO [10] explore sparse or low-rank updates to reduce memory overhead. More recently, MUON [11, 23] employs orthogonalization via Newton-Schulz iteration as a form of preconditioning for matrix parameters. Several variants have emerged [14, 24, 15, 25, 26], including ADAMUON [14] which combines MUON with Adam-style adaptivity, and COSMOS [15] which introduces hybrid mechanisms for memory-efficient training. Studies on full Gauss-Newton methods [5] demonstrate that complete second-order information can substantially improve convergence, motivating the search for practical approximations that balance computational cost with optimization effectiveness.

**Hessian Properties of Neural Networks** Understanding the structure of the Hessian matrix is crucial for designing effective optimization algorithms, as the geometric properties of loss landscapes strongly influence training dynamics [27]. Early spectral analysis [28, 29, 30, 31] revealed that neural network Hessians exhibit a characteristic eigenvalue spectrum: a bulk of near-zero eigenvalues with a small number of isolated large outliers. Subsequent work [32] observed that gradients predominantly align with these outlier eigenvectors during training. Wu et al. [33] further demonstrated that layer-wise Hessians can be approximated using Kronecker factorization, explaining their persistent low-rank structure. Theoretical analyses [34, 35] have provided rigorous explanations for these phenomena, deriving exact formulas for Hessian rank and connecting eigenvalue structure to data properties. Most relevant to our work, Zhang et al. [18] made a significant discovery: the layer-wise Hessian of Transformers exhibits row-wise block-diagonal dominance, where diagonal blocks (corresponding to within-row parameter interactions) have significantly larger magnitudes than off-diagonal blocks (cross-row interactions). This observation has been further investigated by Dong et al. [19], who provide theoretical characterizations of this structured dominance pattern. This row-wise block structure directly motivates our algorithm design, suggesting that row-level preconditioning may suffice to capture essential curvature information while maintaining computational efficiency.

**Convergence Analysis of Adaptive Algorithms** Theoretical understanding of adaptive optimization algorithms in non-convex settings has advanced significantly in recent years. For first-order adaptive methods, Chen et al. [36] established convergence guarantees for ADAM in the non-convex setting, while Li and Lin [37] analyzed RMSPROP and its momentum extension, proving  $O(\sqrt{dT}^{1/4})$  convergence rates measured in  $\ell_1$  norm. A key recent development is the recognition that different optimizers achieve provable advantages under specific geometric structures. Xie et al. [38] demonstrate that ADAM exploits  $\|\cdot\|_{\ell_\infty}$ -smoothness geometry, achieving improved convergence when measured in the dual  $\|\cdot\|_{\ell_1}$  norm. This geometry-dependent analysis has been extended to matrix optimization: Shen et al. [16] and Kim and hwan Oh [17] establish convergence of MUON under nuclear norm smoothness, showing  $O(m)$  complexity compared to the  $O(m^2)$  complexity under Frobenius smoothness. These results reveal that matching the optimizer structure to the problem geometry yields substantial complexity improvements beyond what standard Euclidean or Frobenius analysis would suggest. Information-theoretic lower bounds [20] establish that  $\epsilon^{-4}$  sample complexity is optimal for finding  $\epsilon$ -stationary points in the non-convex stochastic setting, providing fundamental limits for algorithm design.

## 3 Method

### 3.1 RMNP Preconditioner

Recent work reveals that layer-wise Hessians of Transformers exhibit row-wise block-diagonal dominance [18]. As illustrated in Figure 2 (left), diagonal blocks—corresponding to interactions among parameters within the same row—have significantly larger magnitudes than off-diagonal blocks formed by cross-row interactions. This empirical finding is theoretically proven by Dong et al. [19] under specific configurations. Under above condition, the effective curvature of the loss is primarily concentrated on these diagonal blocks.

Preconditioning can be interpreted as correcting the descent direction within an ill-conditioned loss landscape according to the orientation and scale of the landscape’s curvature. Adjustments utilizing the inverse Hessian are regarded as the optimal preconditioner under a quadratic approximation. Meanwhile, the Muon orthogonalized update can be understood as a specific preconditioning method that relies on the outer product of momentum and delivers highly favorable empirical results. By Lemma 4 in Gupta et al. [8], the MUON preconditioner can be characterized in the following form:

$$H_{\text{MUON}} = (V_t V_t^T)^{\frac{1}{2}} \otimes I_n \quad (2)$$

where  $V_t$  denotes the momentum matrix and  $n$  is the column dimension,  $t$  is training step index.

Building on these observations [18], we hypothesize that the dominant curvature information resides in the row-wise diagonal blocks, while cross-row interactions contribute negligibly. This motivates approximating the preconditioner by retaining only diagonal blocks and zeroing out off-diagonal blocks, as shown in Figure 2, yielding the RMNP preconditioner:

$$H_{\text{RMNP}} = \text{diag} \left( (V_t V_t^T)^{\frac{1}{2}} \right) \otimes I_n \quad (3)$$

where  $\text{diag}(\cdot)$  extracts diagonal elements to form a diagonal matrix:  $[\text{diag}(M)]_{ii} = M_{ii}$  and  $[\text{diag}(M)]_{ij} = 0$  for  $i \neq j$ . This structure preserves only the row-wise blocks because  $(V_t V_t^T)_{ii}$  captures interactions within the  $i$ -th row of  $V_t$ , while the Kronecker product  $\text{diag}(\cdot) \otimes I_n$  applies this scaling independently to each row.

The resulting preconditioned update  $\text{diag}(V_t V_t^T)^{-\frac{1}{2}} V_t$  reduces to row-wise  $\ell_2$  normalization:

$$\left[ \text{diag} \left( (V_t V_t^T)^{-\frac{1}{2}} \right) V_t \right]_{i,:} = \frac{V_{t,i,:}}{\sqrt{(V_t V_t^T)_{ii}}} = \frac{V_{t,i,:}}{\|V_{t,i,:}\|_{\ell_2}} \quad (4)$$

where  $V_{t,i,:}$  denotes the  $i$ -th row of  $V_t$  and  $\|V_{t,i,:}\|_{\ell_2} = \sqrt{(V_t V_t^T)_{ii}}$ . This dramatically reduces computational complexity compared to MUON’s Newton-Schulz iteration. The above conjecture is equivalent to implying that the Gram matrix  $V_t V_t^T$  exhibits a certain diagonal dominance property. In the following subsection, we empirically verify this property of the MUON preconditioner.

### 3.2 Analysis of MUON Preconditioner

To investigate the properties of the preconditioner, we analyze the Gram matrix  $V_t V_t^T \in \mathbb{R}^{m \times m}$ , constructed from the matrix parameter  $V_t \in \mathbb{R}^{m \times n}$  at step  $t$ . We define a row-wise metric  $r_i$  to quantify the ratio of the diagonal element to the average magnitude of off-diagonal entries in the  $i$ -th row:

$$r_i \triangleq \frac{(V_t V_t^T)_{ii}}{\frac{1}{m-1} \sum_{j \neq i} |(V_t V_t^T)_{ij}|} = \frac{\|V_{t,i,:}\|_2^2}{\frac{1}{m-1} \sum_{j \neq i} |V_{t,i,:} (V_{t,j,:})^T|} \quad (5)$$

where  $(V_t V_t^T)_{ij}$  denotes the entry at row  $i$  and column  $j$  of the Gram matrix. Based on these row-wise ratios, we introduce the following three aggregate metrics to evaluate the global diagonal dominance across all rows of the matrix. We define *average diagonal dominance ratio* ( $r_{\text{avg}}$ ), *minimum diagonal dominance ratio* ( $r_{\text{min}}$ ) and *maximum diagonal dominance ratio* ( $r_{\text{max}}$ ) as follows:

$$r_{\text{avg}} = \frac{1}{m} \sum_{i=1}^m r_i, \quad r_{\text{min}} = \min_{i \in \{1, \dots, m\}} r_i, \quad r_{\text{max}} = \max_{i \in \{1, \dots, m\}} r_i. \quad (6)$$

Regarding the interpretation, values of  $r_i > 1$  indicate that the diagonal element dominates the average off-diagonal magnitude in row  $i$ , suggesting stronger diagonal dominance. Values approaching 1 suggest that the diagonal element is comparable to the average off-diagonal magnitude, while values significantly greater than 1 indicate that  $V_t V_t^T$  closely approximates a diagonal matrix structure.

To validate our method empirically, we tracked these metrics across all matrix parameters of GPT-2 Small (125M), GPT-2 Medium (355M), and GPT-2 Large (770M) during training. We visualize the evolution of these metrics for 3 randomly selected matrices in Figure 3. Furthermore, we report the global statistics ( $\bar{r}_{\text{avg}}, \bar{r}_{\text{min}}, \bar{r}_{\text{max}}$ ), which average these three statistics across all matrix parameters in the network, in Figure 4. The experimental setup follows that of the previous GPT-2 experiments on OpenWebText; see Appendix D.1 for training hyperparameters and Appendix B for implementation details. Additional LLaMA results are provided in Appendix B; see Figures 9 and 10.

As illustrated in Figure 3, the three representative matrices exhibit strong diagonal dominance, with all three ratio metrics consistently exceeding the baseline of 1 throughout training. For these matrices in GPT-2 Small,  $r_{\text{min}}$  stabilizes above 2,  $r_{\text{avg}}$  exceeds 5, and  $r_{\text{max}}$  reaches approximately 25. Furthermore, the global statistics across all matrices show a similar trend. As shown in Figure 4, the global statistics in GPT-2 Small stabilize at levels indicative of strong diagonal dominance:  $\bar{r}_{\text{min}}$  is approximately 1.6,  $\bar{r}_{\text{avg}}$  is around 4.9, and  $\bar{r}_{\text{max}}$  reaches about 60. It is also worth noting that, in the GPT-2 Medium and Large regimes, the preconditioner exhibits increasingly pronounced diagonal dominance as model size grows. This confirms that the observed diagonal dominance is not an isolated phenomenon but a systematic property of the training dynamics.

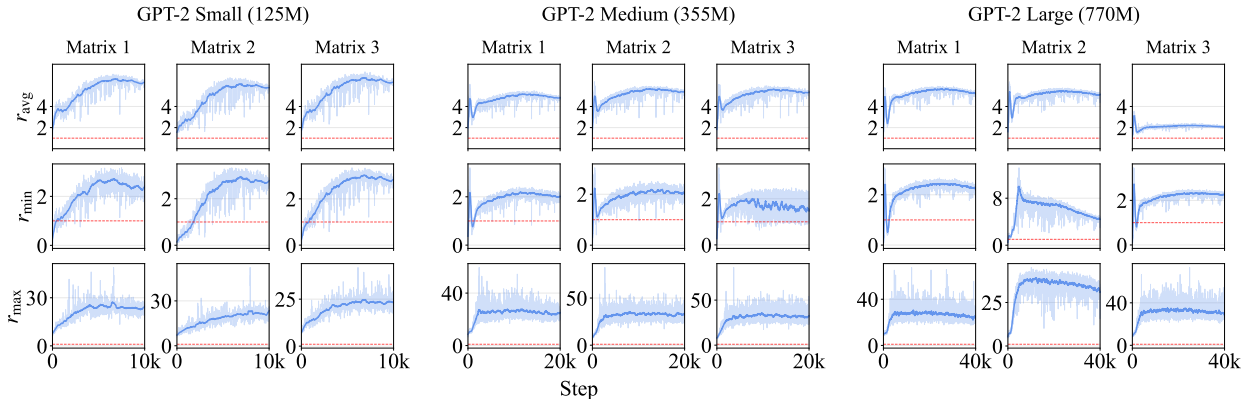


Figure 3: Per-parameter diagonal dominance ratios  $r_{\text{avg}}$ ,  $r_{\text{min}}$ ,  $r_{\text{max}}$  (rows) for three representative matrix parameters (columns) during GPT-2 Small (125M), GPT-2 Medium (355M) and GPT-2 Large (770M) pre-training. Transparent curves: raw values; solid curves: smoothed with window size 50. Red dashed line:  $y = 1$  threshold.

**Discussion with Recent Work** Pethick et al. [39] propose a general framework that unifies various optimizers from a constrained steepest descent perspective. Their work characterizes optimizer updates as steepest descent steps over constrained sets and demonstrates that many existing algorithms, including MUON-like methods, can be recovered through appropriate constraint configurations. Given this generality, it may appear that their framework subsumes RMNP as a special case. However, our work fundamentally differs in motivation. Beyond characterizing row-wise  $\ell_2$ -normalization operation as an instance under an abstract framework, we provide concrete insights into why this specific algorithm works. While Pethick et al. [39] focus on the generality of constrained optimization viewpoints, our approach stems directly from preconditioning principles that leverage the intrinsic row-wise block-diagonal dominance observed in neural network Hessians. Rather than deriving row normalization as an instance of abstract constrained steepest descent, we explain *why* row normalization functions as an effective preconditioning mechanism for neural networks. Our contribution

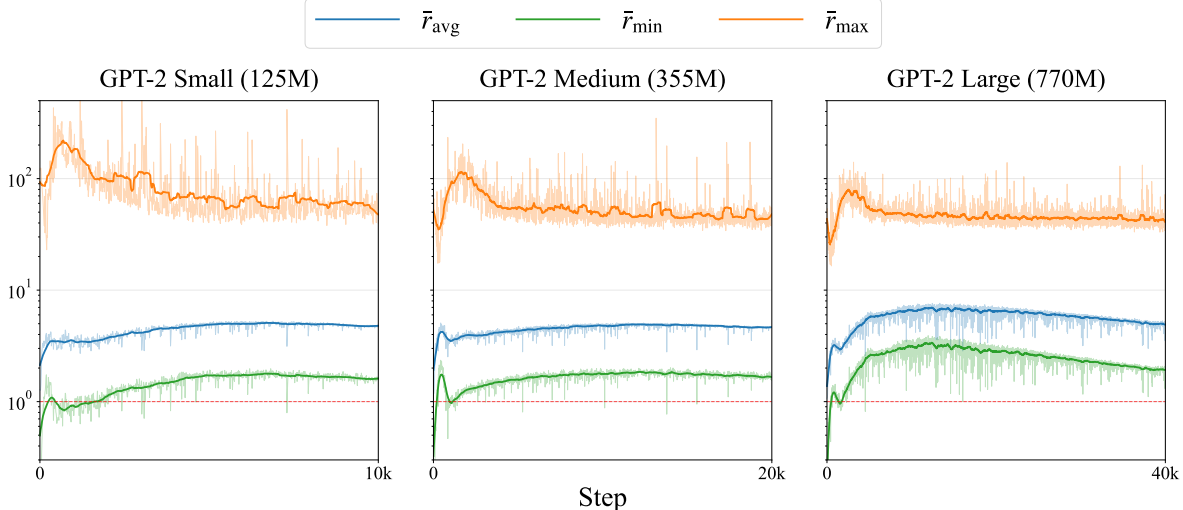


Figure 4: Global diagonal dominance ratios  $\bar{r}_{\text{avg}}$ ,  $\bar{r}_{\text{min}}$ ,  $\bar{r}_{\text{max}}$  averaged across all matrix parameters during GPT-2 Small (125M), GPT-2 Medium (355M), and GPT-2 Large (770M) pre-training. Y-axis in log scale. Transparent curves: raw values; solid curves: smoothed with window size 50. Red dashed line:  $y = 1$  threshold. The metrics quickly rise above 1 after warm-up and remain mostly above 1, confirming strong diagonal dominance during training.

lies in explicitly connecting this operation to the geometric structure of neural network curvature, supported by both empirical observations of diagonal dominance and theoretical convergence guarantees.

## 4 Main Experimental Results

In this section, we demonstrate that RMNP achieves competitive optimization performance while maintaining high computational efficiency. We first show that RMNP reduces the preconditioning computational cost by an order of magnitude compared to MUON, demonstrating its scalability advantages. We then evaluate RMNP against ADAMW and MUON, two prevalent optimizers for training large language models, on the GPT-2 and LLaMA model series. GPT-2 models are trained on OpenWebText [40] and FineWeb-Edu-100B [41], while LLaMA models are trained on C4 [42].

### 4.1 Experimental Setup

**MUON** Following the setup in Jordan et al. [11], Liu et al. [23], we employ a mixed update strategy where matrix parameters are optimized using MUON and non-matrix parameters using ADAMW. We introduce two distinct learning rate hyperparameters,  $\text{lr}_{\text{AdamW}}$  and  $\text{lr}_{\text{Matrix}}$ , both following a cosine annealing schedule with a 10% warmup period.

**RMNP** For RMNP, we align our experimental setup with the MUON protocol described above. We employ an almost identical mixed update strategy, applying RMNP to matrix parameters and ADAMW to non-matrix parameters. Similarly, we utilize two learning rates,  $\text{lr}_{\text{AdamW}}$  and  $\text{lr}_{\text{Matrix}}$ , both subject to a cosine annealing schedule with a 10% warmup. Consistent with the baseline settings, we fix the ADAMW hyperparameters ( $\beta = (0.9, 0.95)$ , weight decay 0.1) and exclusively tune the learning rate for the matrix optimizer,  $\text{lr}_{\text{Matrix}}$ , during the search process.

**ADAMW** For the ADAMW setup, we follow the standard setup in Yuan et al. [43] for training GPT-2, and He et al. [44] for LLaMA. We set  $\beta = (0.9, 0.95)$  and weight decay 0.1, and a cosine annealing schedule with 10% warm up which consistent with the ADAMW configuration used in the mixed update strategy above.

**GPT-2 Pre-Training on OpenWebText** Experiments on GPT-2 are conducted based on the implementation of Yuan et al. [43], using the OpenWebText dataset [40] and the GPT-2 tokenizer. We pretrain three scales of GPT-2 models: small (125M parameters), medium (355M parameters), and large (770M parameters). For model configurations, we set the dropout rate to 0.0 and disable biases. Training hyperparameters are listed in Tables 5 and 9 in Appendix D.2. We also evaluate on FineWeb-Edu-100B [41, 45] across three GPT-2 scales (Small, Medium, and Large); see Appendix D.2 for configurations and results.

**LLaMA Pre-Training on C4** Experiments on LLaMA are conducted on the C4 dataset [42]. We pretrain three scales of LLaMA models: LLaMA-60M, LLaMA-130M and LLaMA-350M. Training hyperparameters are listed in Table 9 in Appendix D.2.

Table 2: Efficiency comparison between MUON and RMNP’s preconditioning cost on GPT-2 models. Time measured over 100 steps with batch size 16 on a single RTX Pro 6000 GPU.

Size	Time Cost (s)		Speedup ( $\times$ )
	MUON	RMNP	
60M	1.480	<b>0.115</b>	12.9
125M	2.975	<b>0.201</b>	14.8
200M	4.140	<b>0.260</b>	15.9
355M	7.380	<b>0.401</b>	18.4
500M	15.720	<b>0.462</b>	34.0
770M	27.070	<b>0.611</b>	44.3
1.3B	30.570	<b>0.783</b>	39.0
1.5B	36.650	<b>0.855</b>	42.9

## 4.2 Preconditioning Time Cost

Since RMNP and MUON primarily differ in their choice of preconditioner, where MUON applies Newton–Schulz orthogonalization whereas RMNP uses row normalization, we benchmark the preconditioner-operator overhead of RMNP against MUON. Specifically, we report the per-iteration time attributable to the preconditioner operator (*Step Time*) and the cumulative time over 100 iterations (*Total Time*). Experiments are run on GPT-2 models ranging from 60M to 1.5B parameters with a batch size of 16. See Appendix C.1 for detailed model configurations.

As shown in Table 2, RMNP achieves significant speedup over MUON across all model sizes. The row normalization in RMNP is approximately 13–44 $\times$  faster than the Newton–Schulz orthogonalization in MUON. This result underscores RMNP’s computational efficiency. More importantly, as model size grows and Newton–Schulz orthogonalization increasingly becomes the dominant bottleneck in end-to-end training throughput, RMNP’s lightweight preconditioner offers a more scalable alternative, indicating strong potential for training at very large scale. For example, in Table 2, for GPT-2 125M, MUON’s preconditioning cost per 100 steps is only 1.48 seconds, and RMNP provides an 12.9 $\times$  speedup. However, for GPT-2 1.5B, the preconditioning cost per 100 steps increases to 36.65 seconds, while RMNP achieves a 42.9 $\times$  speedup. See Appendix C for detailed results including memory usage.

### 4.3 Pretraining Performance

**RMNP consistently outperforms MUON and ADAMW in GPT-2 experiments.** As shown in Figure 5, across the Small, Medium, and Large settings, while efficiently reducing the preconditioner-operator overhead, RMNP still delivers more competitive results than both baselines in terms of evaluation perplexity: on the Small setting it improves over MUON by 0.04 and over ADAMW by 1.37; on the Medium setting the improvements are 0.07 and 1.49; and on the Large setting they are 0.24 and 0.84, respectively. This consistent pattern suggests that RMNP’s efficiency gains in Table 2 do not come at the expense of optimization quality; instead, it preserves strong optimization behavior while reducing preconditioning overhead, yielding a favorable speed–accuracy trade-off across model scales under a standard large-model training protocol. Our GPT-2 experiments on OpenWebText match the results reported in Yuan et al. [43]. We conduct an extensive hyperparameter grid search for both MUON and RMNP; see Table 10 and 11 in Appendix D. Results on FineWeb-Edu-100B further confirm this trend (Appendix D.2).

**RMNP consistently outperforms MUON and ADAMW in LLaMA experiments.** As shown in Figure 6, RMNP consistently achieves comparable perplexity to MUON across all model sizes, while maintaining a slight performance edge. Specifically, RMNP demonstrates modest improvements over the baseline: on the LLaMA-60M setting, it decreases perplexity by 0.63 compared to MUON and 4.33 compared to ADAMW; on the LLaMA-130M setting, the gain is 0.28 over MUON and 1.10 compared to ADAMW; and on the LLaMA-350M setting, the improvement is 0.02 over MUON. This pattern suggests that RMNP is able to fully match the optimization quality of MUON without the heavy preconditioning overhead, effectively delivering efficiency gains without sacrificing performance. It is worth noting that we perform a systematic hyperparameter grid search for both MUON and RMNP; see Table 12, 13 and 14 in Appendix D.

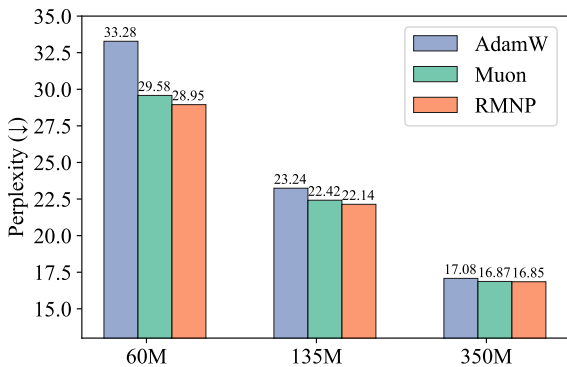
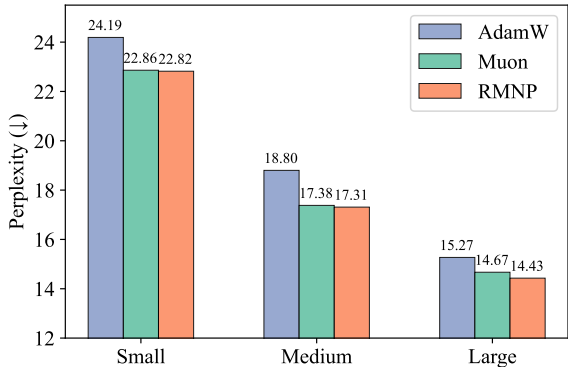


Figure 5: Results for GPT-2 on OpenWebText: Small (125M) trained with 5B tokens; Medium (355M) trained with 10B tokens, and Large (770M) trained with 20B tokens. FineWeb-Edu-100B results are in Figure 11.

Figure 6: Results for LLaMA: 60M trained with 1B tokens; 130M trained with 2B tokens, and 350M trained with 6B tokens.

## 5 Non-Convex Convergence

In this section, we present the convergence analysis of our proposed method under the non-convex smooth setting. Our setup is consistent with many existing analyses for adaptive algorithms [36, 38, 37, 16, 17], assuming only the smoothness of the loss function, alongside unbiased stochastic gradients and bounded second moments, as detailed in Section 5.2.

Recent work reveals that optimizers can achieve provable advantages under specific geometric structures beyond standard  $\ell_2$  or Frobenius smoothness. For instance, Xie et al. [38] discuss benefits of ADAM under  $\|\cdot\|_{\ell_\infty}$ -smoothness with convergence measured in  $\|\cdot\|_{\ell_1}$ , while Shen et al. [16], Kim and hwan Oh [17] establish advantages of MUON under  $\|\cdot\|_2$ -smoothness with convergence measured in nuclear norm. Similarly,

we identify the geometric structure under which RMNP achieves provable benefits. We establish three convergence results: under the standard  $\|\cdot\|_F$ -smoothness assumption, we prove convergence in both the Frobenius norm sense (Theorem 5.5) and the  $\|\cdot\|_{1,2}$  norm sense (Theorem 5.7). More importantly, under the  $\|\cdot\|_{\infty,2}$ -smoothness assumption, we establish improved convergence guarantees in the  $\|\cdot\|_{1,2}$  norm sense (Theorem 5.9), revealing that RMNP similarly benefits from its matched geometric structure.

## 5.1 Notation

Let  $W \in \mathbb{R}^{m \times n}$  denote the parameter matrix, where  $W_{i,:} \in \mathbb{R}^n$  denotes the  $i$ -th row. The matrix inner product is  $\langle Z, W \rangle = \text{Tr}(Z^\top W)$ . We use the Frobenius norm  $\|W\|_F = \sqrt{\sum_{i,j} W_{i,j}^2}$ , the mixed norm  $\|W\|_{1,2} = \sum_{i=1}^m \|W_{i,:}\|_2$ , and the norm  $\|W\|_{\infty,2} = \max_{i=1,\dots,m} \|W_{i,:}\|_2$ . These satisfy the duality  $|\langle A, B \rangle| \leq \|A\|_{1,2} \|B\|_{\infty,2}$ . We use  $\mathbb{E}[\cdot]$  to denote the expectation and  $\mathbb{E}_t[\cdot | \mathcal{F}_{t-1}]$  to denote the conditional expectation given  $\mathcal{F}_{t-1}$ . Since the input dimension is generally smaller than the output dimension in neural networks, without loss of generality, we assume  $m < n$  throughout this discussion.

## 5.2 Assumptions

**Assumption 5.1** (Lipschitz Gradient). The gradient of  $f : \mathbb{R}^{m \times n} \rightarrow \mathbb{R}$  is Lipschitz continuous in one of the following norms:

(a) *Frobenius norm*: There exists  $L_F > 0$  such that for all  $W, W' \in \mathbb{R}^{m \times n}$ ,

$$\|\nabla f(W) - \nabla f(W')\|_F \leq L_F \|W - W'\|_F.$$

(b) *(1,2)-norm with respect to  $(\infty,2)$ -norm*: There exists  $L_{\infty,2} > 0$  such that for all  $W, W' \in \mathbb{R}^{m \times n}$ ,

$$\|\nabla f(W) - \nabla f(W')\|_{(1,2)} \leq L_{\infty,2} \|W - W'\|_{\infty,2}.$$

**Assumption 5.2** (Unbiased Gradient Estimator). For all  $t$  and  $W_t$ ,

$$\mathbb{E}_t[G_t | \mathcal{F}_{t-1}] = \mathbb{E}_t[\nabla f(W_t; \xi^t) | \mathcal{F}_{t-1}] = \nabla f(W_t).$$

**Assumption 5.3** (Bounded Gradient Variance). There exists a constant  $\sigma > 0$  such that for all  $t$  and  $W_t$ ,

$$\mathbb{E}_t[\|G_t - \nabla f(W_t)\|_F^2 | \mathcal{F}_{t-1}] \leq \frac{\sigma^2}{B},$$

where  $B$  is the batch size (i.e., the number of samples used to compute  $G_t$ ).

**Assumption 5.4** (Lower Bound).  $f$  is bounded below with  $f^* = \inf_W f(W)$ . Define  $\Delta = f(W_0) - f^*$ .

## 5.3 Main Results

We now present our main theoretical results, which establish convergence guarantees for RMNP under different smoothness assumptions and convergence criteria. Our analysis reveals how the choice of matrix norms—both in the smoothness assumption and in the convergence measure—affects the sample complexity.

**Theorem 5.5** ( $\|\cdot\|_F$ - Lipschitz). *Under Assumptions 5.1(a), 5.2, 5.3, and 5.4, if Algorithm 2 uses constant  $\eta_t = \eta$  and momentum  $\beta \in [0, 1)$ , then*

$$\frac{1}{T} \sum_{t=1}^T \mathbb{E}[\|\nabla f(W_t)\|_F] \leq \frac{\Delta}{T\eta} + (\sqrt{m} + 1) \left[ \left(1 - \frac{1}{T}\right) \frac{L_F \eta \sqrt{m} \beta}{1 - \beta} + \frac{\sigma}{\sqrt{B}} \sqrt{\frac{1 - \beta}{1 + \beta}} \right] + \frac{L_F \eta m}{2}. \quad (7)$$

*Remark 5.6* (Complexity for Theorem 5.5). If we set  $B = 1$ ,  $\eta = \sqrt{\frac{(1-\beta)\Delta}{L_F m T}}$ , and  $1 - \beta = \min \left\{ \frac{\sqrt{L_F \Delta}}{(\sqrt{m+1})\sigma\sqrt{T}}, 1 \right\}$ , then the bound in (7) yields

$$\frac{1}{T} \sum_{t=1}^T \mathbb{E} [\|\nabla f(W_t)\|_F] \leq O \left( \sqrt[4]{\frac{m^2 L_F \Delta \sigma^2}{T}} + \sqrt{\frac{L_F m \Delta}{T}} + \frac{m \sigma^2}{\sqrt{L_F \Delta T}} \right).$$

Thus, we can find an  $\epsilon$ -stationary point (in Frobenius norm) of  $f$  with a complexity of  $O(m^2 L_F \sigma^2 \Delta \epsilon^{-4})$ , exhibiting an  $O(m^2)$  dimension dependence.

The detailed proof of Theorem 5.5 can be found in Appendix A.4. While Theorem 5.5 establishes convergence in the Frobenius norm, matrix optimization problems often involve alternative matrix norms that better capture the underlying structure. Our next result analyzes convergence in the  $\|\cdot\|_{1,2}$  norm under the same Frobenius smoothness assumption, demonstrating that RMNP achieves comparable complexity guarantees across different convergence measures.

**Theorem 5.7** ( $\|\cdot\|_{1,2}$ -Convergence under  $\|\cdot\|_F$ -Lipschitz). *Under Assumptions 5.1(a), 5.2, 5.3, and 5.4, if Algorithm 2 uses constant  $\eta_t = \eta$  and momentum  $\beta \in [0, 1)$ , then*

$$\frac{1}{T} \sum_{t=1}^T \mathbb{E} [\|\nabla f(W_t)\|_{1,2}] \leq \frac{\Delta}{T\eta} + 2 \left[ \left(1 - \frac{1}{T}\right) \frac{L_F \eta m \beta}{1 - \beta} + \frac{\sqrt{m}\sigma}{\sqrt{B}} \sqrt{\frac{1 - \beta}{1 + \beta}} \right] + \frac{L_F \eta m}{2}. \quad (8)$$

*Remark 5.8* (Complexity for Theorem 5.7). If we set  $B = 1$ ,  $\eta = \sqrt{\frac{(1-\beta)\Delta}{L_F m T}}$ , and

$$1 - \beta = \min \left\{ \frac{\sqrt{L_F \Delta}}{2\sqrt{m}\sigma\sqrt{T}}, 1 \right\},$$

then the bound in (8) yields

$$\frac{1}{T} \sum_{t=1}^T \mathbb{E} [\|\nabla f(W_t)\|_{1,2}] \leq O \left( \sqrt[4]{\frac{m^2 L_F \Delta \sigma^2}{T}} + \sqrt{\frac{L_F m \Delta}{T}} + \frac{m \sigma^2}{\sqrt{L_F \Delta T}} \right).$$

Thus, we can find an  $\epsilon$ -stationary point (in  $\|\cdot\|_{1,2}$  norm) of  $f$  with a complexity of  $O(m^2 L_F \sigma^2 \Delta \epsilon^{-4})$ , exhibiting an  $O(m^2)$  dimension dependence.

The detailed proof of Theorem 5.7 can be found in Appendix A.4. The preceding results demonstrate that under Frobenius smoothness, both convergence measures achieve  $O(m^2)$  complexity. However, when the objective function exhibits a different geometric structure—specifically, when the gradient is Lipschitz continuous with respect to the  $\|\cdot\|_{\infty,2}$  norm—RMNP’s row normalization operation can exploit this structure more effectively. Our final result establishes a significantly improved complexity bound in this setting.

**Theorem 5.9** ( $\|\cdot\|_{1,2}$ -Lipschitz). *Under Assumptions 5.1(b), 5.2, 5.3, and 5.4, if Algorithm 2 uses constant  $\eta_t = \eta$  and momentum  $\beta \in [0, 1)$ , then*

$$\frac{1}{T} \sum_{t=1}^T \mathbb{E} [\|\nabla f(W_t)\|_{1,2}] \leq \frac{\Delta}{T\eta} + 2 \left[ \left(1 - \frac{1}{T}\right) \frac{L_{\infty,2} \eta \beta}{1 - \beta} + \frac{\sqrt{m}\sigma}{\sqrt{B}} \sqrt{\frac{1 - \beta}{1 + \beta}} \right] + \frac{L_{\infty,2} \eta}{2}. \quad (9)$$

*Remark 5.10* (Complexity for Theorem 5.9). If we set  $B = 1$ ,  $\eta = \sqrt{\frac{(1-\beta)\Delta}{L_{\infty,2} T}}$ , and  $1 - \beta = \min \left\{ \frac{\sqrt{L_{\infty,2} \Delta}}{2\sqrt{m}\sigma\sqrt{T}}, 1 \right\}$ , then the bound in (9) yields

$$\frac{1}{T} \sum_{t=1}^T \mathbb{E} [\|\nabla f(W_t)\|_{1,2}] \leq O \left( \sqrt[4]{\frac{m L_{\infty,2} \Delta \sigma^2}{T}} + \sqrt{\frac{L_{\infty,2} \Delta}{T}} + \frac{\sqrt{m}\sigma^2}{\sqrt{L_{\infty,2} \Delta T}} \right).$$

Thus, we can find an  $\epsilon$ -stationary point (in  $\|\cdot\|_{1,2}$  norm) of  $f$  with a complexity of  $O(m L_{\infty,2} \sigma^2 \Delta \epsilon^{-4})$ .

The detailed proof of Theorem 5.9 can be found in Appendix A.4.

## 5.4 Comparison with Related Work

We now compare our theoretical results with recent work on MUON optimizers, as summarized in Table 1. Similar to MUON, RMNP demonstrates geometry-dependent advantages: different smoothness assumptions lead to different convergence guarantees. Under Frobenius norm smoothness (Assumption 5.1(a)), both Theorem 5.5 and Theorem 5.7 achieve a sample complexity of  $O(m^2 L_F \sigma^2 \Delta \epsilon^{-4})$ , matching the recent results for MUON [16]. More importantly, under the  $\|\cdot\|_{\infty,2}$ -smoothness assumption (Assumption 5.1(b)), Theorem 5.9 achieves an improved complexity of  $O(m L_{\infty,2} \sigma^2 \Delta \epsilon^{-4})$ , representing a quadratic improvement in dimension dependence from  $O(m^2)$  to  $O(m)$ . This mirrors MUON’s improvement under nuclear norm smoothness, where convergence of  $\|\nabla f\|_*$  also achieves  $O(m)$  complexity [16]. Although the geometric structures differ—MUON exploits nuclear norm geometry while RMNP exploits  $\|\cdot\|_{1,2}$  geometry—both methods achieve the same  $O(m)$  dimension dependence in their respective favorable settings. This improvement stems from RMNP’s row normalization operation, which naturally aligns with the row-wise structure present in the  $\|\cdot\|_{1,2}$  geometry.

## 6 Conclusion

In this paper, we introduced **RMNP** (Row Momentum Normalized Preconditioning), an efficient optimizer that significantly advances preconditioned adaptive methods for deep neural network training. Motivated by the diagonal block dominance structure observed in Transformer Hessians, RMNP replaces the Newton-Schulz iteration in MUON with a simple row-wise  $\ell_2$  normalization operation, reducing the per-iteration computational complexity from  $\mathcal{O}(mn \cdot \min(m, n))$  to  $\mathcal{O}(mn)$ —an order of magnitude improvement.

Our contributions span three key dimensions. **Algorithmically**, RMNP achieves substantial efficiency gains, delivering 13–44× speedup **on the preconditioning process** over MUON across model scales from 60M to 1.5B parameters while maintaining comparable memory usage. **Empirically**, extensive experiments on GPT-2 (125M, 355M, 770M) and LLaMA (60M, 130M, 350M) demonstrate that RMNP consistently matches or outperforms both MUON and AdamW in terms of final performance. Our empirical analysis validates the diagonal dominance property of the MUON preconditioner, providing strong support for RMNP’s design principle. We also provide practical hyperparameter recommendations, showing that  $\text{lr}_{\text{Matrix}}$  is the primary factor influencing performance. **Theoretically**, we establish rigorous convergence guarantees in the non-convex setting that match recent results for MUON optimizers. As summarized in Table 1, RMNP achieves sample complexity of  $O(m^2 L_F \sigma^2 \Delta \epsilon^{-4})$  under Frobenius smoothness and an improved  $O(m L_{\infty,2} \sigma^2 \Delta \epsilon^{-4})$  under  $\|\cdot\|_{\infty,2}$ -smoothness, and both results’ complexity achieving information-theoretic minimax optimality [20].

By effectively balancing preconditioning effectiveness with computational efficiency, RMNP provides a more scalable preconditioning approach that becomes particularly advantageous when MUON’s preconditioning process emerges as a computational bottleneck in large-scale training scenarios.

## Acknowledgments

We thank our collaborators, colleagues, and funding agencies. This work is supported by the DARPA AIQ program, the U.S. Department of Energy under Award Number DE-SC0025584, Dartmouth College, and Lambda AI.

## References

- [1] John Duchi, Elad Hazan, and Yoram Singer. Adaptive subgradient methods for online learning and stochastic optimization. *Journal of Machine Learning Research*, 12(61):2121–2159, 2011.
- [2] Tijmen Tieleman and Geoffrey Hinton. Lecture 6.5-rmsprop: Divide the gradient by a running average of its recent magnitude. *COURSERA: Neural networks for machine learning*, 4(2):26–31, 2012.

- [3] Diederik P Kingma and Jimmy Ba. Adam: A method for stochastic optimization. *arXiv preprint arXiv:1412.6980*, 2014.
- [4] Ilya Loshchilov and Frank Hutter. Decoupled weight decay regularization. In *International Conference on Learning Representations*, 2019.
- [5] Natalie Abreu, Nikhil Vyas, Sham M. Kakade, and Depen Morwani. The potential of second-order optimization for LLMs: A study with full Gauss-Newton. *arXiv preprint arXiv:2510.09378*, 2025.
- [6] James Martens and Roger Grosse. Optimizing neural networks with Kronecker-factored approximate curvature. In *International Conference on Machine Learning (ICML)*, volume 37 of *Proceedings of Machine Learning Research*, pages 2408–2417. PMLR, 2015.
- [7] Xi-Lin Li. Preconditioned stochastic gradient descent. *IEEE Transactions on Neural Networks and Learning Systems*, 29(5):1454–1466, 2018.
- [8] Vineet Gupta, Tomer Koren, and Yoram Singer. Shampoo: Preconditioned stochastic tensor optimization. In *International Conference on Machine Learning (ICML)*, volume 80 of *Proceedings of Machine Learning Research*, pages 1842–1850. PMLR, 2018.
- [9] Yi Ren, Achraf Bahamou, and Donald Goldfarb. Kronecker-factored quasi-newton methods for deep learning. *arXiv preprint arXiv:2102.06737*, 2021.
- [10] Kang An, Yuxing Liu, Rui Pan, Yi Ren, Shiqian Ma, Donald Goldfarb, and Tong Zhang. ASGO: Adaptive structured gradient optimization. In *The Thirty-ninth Annual Conference on Neural Information Processing Systems*, 2025. URL <https://openreview.net/forum?id=fru52tkjHf>.
- [11] Keller Jordan, Yuchen Jin, Vlado Boza, Jiacheng You, Franz Cesista, Laker Newhouse, and Jeremy Bernstein. Muon: An optimizer for hidden layers in neural networks. <https://kellerjordan.github.io/posts/muon/>, 2024.
- [12] Ran Tian and Ankur P. Parikh. Amos: An Adam-style optimizer with adaptive weight decay towards model-oriented scale. *arXiv preprint arXiv:2210.11693*, 2022.
- [13] Nikhil Vyas, Depen Morwani, Rosie Zhao, Itai Shapira, David Brandfonbrener, Lucas Janson, and Sham M. Kakade. SOAP: Improving and stabilizing shampoo using adam for language modeling. In *The Thirteenth International Conference on Learning Representations*, 2025. URL <https://openreview.net/forum?id=IDxZhXrpNf>.
- [14] Chongjie Si, Daquan Zhang, and Wei Shen. AdaMuon: Adaptive Muon optimizer. *arXiv preprint arXiv:2507.11005*, 2025.
- [15] Liming Liu, Zhenghao Xu, Zixuan Zhang, Hao Kang, Zichong Li, Chen Liang, Weizhu Chen, and Tuo Zhao. COSMOS: A hybrid adaptive optimizer for memory-efficient training of LLMs. *arXiv preprint arXiv:2502.17410*, 2025.
- [16] Wei Shen, Ruichuan Huang, Minhui Huang, Cong Shen, and Jiawei Zhang. On the convergence analysis of muon. *arXiv preprint arXiv:2505.23737*, 2025.
- [17] Gyu Yeol Kim and Min hwan Oh. Convergence of muon with newton-schulz, 2026. URL <https://arxiv.org/abs/2601.19156>.
- [18] Yushun Zhang, Congliang Chen, Tian Ding, Ziniu Li, Ruoyu Sun, and Zhiqian Luo. Why transformers need adam: A hessian perspective. *Advances in neural information processing systems*, 37:131786–131823, 2024.
- [19] Zhaorui Dong, Yushun Zhang, Jianfeng Yao, and Ruoyu Sun. Towards quantifying the hessian structure of neural networks. *arXiv preprint arXiv:2505.02809*, 2025.

- [20] Yossi Arjevani, Yair Carmon, John C Duchi, Dylan J Foster, Nathan Srebro, and Blake Woodworth. Lower bounds for non-convex stochastic optimization. *Mathematical Programming*, 199(1):165–214, 2023.
- [21] Xi-Lin Li. Black box lie group preconditioners for sgd. *arXiv preprint arXiv:2211.04422*, 2022.
- [22] Hao-Jun Michael Shi, Tsung-Hsien Lee, Shintaro Iwasaki, Jose Gallego-Posada, Zhijing Li, Kaushik Rangadurai, Dheevatsa Mudigere, and Michael Rabbat. A distributed data-parallel PyTorch implementation of the distributed Shampoo optimizer for training neural networks at-scale. *arXiv preprint arXiv:2309.06497*, 2023.
- [23] Jingyuan Liu, Jianlin Su, Xingcheng Yao, Zhejun Jiang, Guokun Lai, Yulun Du, Yidao Qin, Weixin Xu, Enzhe Lu, Junjie Yan, et al. Muon is scalable for LLM training. *arXiv preprint arXiv:2502.16982*, 2025.
- [24] Zichong Li, Liming Liu, Chen Liang, Weizhu Chen, and Tuo Zhao. Normuon: Making muon more efficient and scalable. *arXiv preprint arXiv:2510.05491*, 2025.
- [25] Kaiyue Wen, David Hall, Tengyu Ma, and Percy Liang. Fantastic pretraining optimizers and where to find them. *arXiv preprint arXiv:2509.02046*, 2025.
- [26] Tianyu Pang, Yujie Fang, Zihang Liu, Shenyang Deng, Lei Hsiung, Shuhua Yu, and Yaoqing Yang. Htmuon: Improving muon via heavy-tailed spectral correction, 2026. URL <https://arxiv.org/abs/2603.10067>.
- [27] Hao Li, Zheng Xu, Gavin Taylor, Christoph Studer, and Tom Goldstein. Visualizing the loss landscape of neural nets. *Advances in Neural Information Processing Systems*, 31, 2018.
- [28] Levent Sagun, Léon Bottou, and Yann LeCun. Eigenvalues of the Hessian in deep learning: Singularity and beyond. *arXiv preprint arXiv:1611.07476*, 2016.
- [29] Levent Sagun, Utku Evci, V Ugur Guney, Yann Dauphin, and Leon Bottou. Empirical analysis of the Hessian of over-parametrized neural networks. *arXiv preprint arXiv:1706.04454*, 2017.
- [30] Shenyang Deng, Boyao Liao, Zhuoli Ouyang, Tianyu Pang, Minhak Song, and Yaoqing Yang. Suspicious alignment of sgd: A fine-grained step size condition analysis, 2026. URL <https://arxiv.org/abs/2601.11789>.
- [31] Shenyang Deng, Boyao Liao, Zhuoli Ouyang, Tianyu Pang, and Yaoqing Yang. Depth, not data: An analysis of hessian spectral bifurcation, 2026. URL <https://arxiv.org/abs/2602.00545>.
- [32] Behrooz Ghorbani, Shankar Krishnan, and Ying Xiao. An investigation into neural net optimization via hessian eigenvalue density. In *International Conference on Machine Learning*, pages 2232–2241. PMLR, 2019.
- [33] Yikai Wu, Xingyu Zhu, Chenwei Wu, Annie Wang, and Rong Ge. Dissecting Hessian: Understanding common structure of Hessian in neural networks. In *Advances in Neural Information Processing Systems*, volume 33, pages 10193–10204, 2020.
- [34] Sidak Pal Singh, Gregor Bachmann, and Thomas Hofmann. Analytic insights into structure and rank of neural network Hessian maps. *Advances in Neural Information Processing Systems*, 34:23914–23927, 2021.
- [35] Zhenyu Liao and Michael W Mahoney. Hessian eigenspectra of more realistic nonlinear models. *Advances in Neural Information Processing Systems*, 34:20104–20117, 2021.
- [36] Congliang Chen, Li Shen, Fangyu Zou, and Wei Liu. Towards practical adam: Non-convexity, convergence theory, and mini-batch acceleration. *Journal of Machine Learning Research*, 23(229):1–47, 2022.

- [37] Huan Li and Zhouchen Lin. On the  $o(\sqrt{dt}^{1/4})$  convergence rate of RMSProp and its momentum extension measured by  $\ell_1$  norm. *arXiv preprint arXiv:2402.00389*, 2024.
- [38] Shuo Xie, Mohamad Amin Mohamadi, and Zhiyuan Li. Adam exploits  $\ell_\infty$ -geometry of loss landscape via coordinate-wise adaptivity. In *The Thirteenth International Conference on Learning Representations*, 2025. URL <https://openreview.net/forum?id=PUnD86UEK5>.
- [39] Thomas Pethick, Wanyun Xie, Kimon Antonakopoulos, Zhenyu Zhu, Antonio Silveti-Falls, and Volkan Cevher. Training deep learning models with norm-constrained LMOs. In *Forty-second International Conference on Machine Learning*, 2025. URL <https://openreview.net/forum?id=20qm2IzTy9>.
- [40] Aaron Gokaslan, Vanya Cohen, Ellie Pavlick, and Stefanie Tellex. Openwebtext corpus. <http://Skylion007.github.io/OpenWebTextCorpus>, 2019.
- [41] Guilherme Penedo, Hynek Kydlíček, Loubna Ben allal, Anton Lozhkov, Margaret Mitchell, Colin Raffel, Leandro Von Werra, and Thomas Wolf. The fineweb datasets: Decanting the web for the finest text data at scale, 2024. URL <https://arxiv.org/abs/2406.17557>.
- [42] Colin Raffel, Noam Shazeer, Adam Roberts, Katherine Lee, Sharan Narang, Michael Matena, Yanqi Zhou, Wei Li, and Peter J Liu. Exploring the limits of transfer learning with a unified text-to-text transformer. *Journal of machine learning research*, 21(140):1–67, 2020.
- [43] Huizhuo Yuan, Yifeng Liu, Shuang Wu, Zhou Xun, and Quanquan Gu. MARS: Unleashing the power of variance reduction for training large models. In *Forty-second International Conference on Machine Learning*, 2025. URL <https://openreview.net/forum?id=NrcKQ3ASLZ>.
- [44] Di He, Songjun Tu, Ajay Jaiswal, Li Shen, Ganzhao Yuan, Shiwei Liu, and Lu Yin. Alphadecay: Module-wise weight decay for heavy-tailed balancing in llms. *arXiv preprint arXiv:2506.14562*, 2025.
- [45] Andrej Karpathy. Fineweb-edu-100b-shuffle. <https://huggingface.co/datasets/karpathy/fineweb-edu-100b-shuffle>, 2024.

## A Proof of Theorem

### A.1 Notation

We first recall our notation here, Let  $W \in \mathbb{R}^{m \times n}$  denote the parameter matrix, where  $W_{i,:} \in \mathbb{R}^n$  denotes the  $i$ -th row. The matrix inner product is  $\langle Z, W \rangle = \text{Tr}(Z^\top W)$ . We use the Frobenius norm  $\|W\|_F = \sqrt{\sum_{i,j} W_{i,j}^2}$ , the mixed norm  $\|W\|_{1,2} = \sum_{i=1}^m \|W_{i,:}\|_2$ , and the norm  $\|W\|_{\infty,2} = \max_{i=1,\dots,m} \|W_{i,:}\|_2$ . These satisfy the duality  $|\langle A, B \rangle| \leq \|A\|_{1,2} \|B\|_{\infty,2}$ . We use  $\mathbb{E}[\cdot]$  to denote the expectation and  $\mathbb{E}_t[\cdot | \mathcal{F}_{t-1}]$  to denote the conditional expectation given  $\mathcal{F}_{t-1}$ .

### A.2 Assumptions

*Assumption (Lipschitz Gradient).* The gradient of  $f : \mathbb{R}^{m \times n} \rightarrow \mathbb{R}$  is Lipschitz continuous in one of the following norms:

(a) *Frobenius norm:* There exists a constant  $L_F > 0$  such that for all  $W, W' \in \mathbb{R}^{m \times n}$ ,

$$\|\nabla f(W) - \nabla f(W')\|_F \leq L_F \|W - W'\|_F.$$

(b) *Mixed norm:* There exists a constant  $L_{\infty,2} > 0$  such that for all  $W, W' \in \mathbb{R}^{m \times n}$ ,

$$\|\nabla f(W) - \nabla f(W')\|_{1,2} \leq L_{\infty,2} \|W - W'\|_{\infty,2}.$$

*Assumption (Unbiased Estimator).* For all iterations  $t$  and all parameter values  $W_t$ ,

$$\mathbb{E}_t[G_t | \mathcal{F}_{t-1}] = \nabla f(W_t).$$

*Assumption (Bounded Variance).* There exists a constant  $\sigma > 0$  such that for all iterations  $t$  and all parameter values  $W_t$ ,

$$\mathbb{E}_t[\|G_t - \nabla f(W_t)\|_F^2 | \mathcal{F}_{t-1}] \leq \frac{\sigma^2}{B},$$

where  $B$  is the batch size.

*Assumption (Lower Bound).* The objective function  $f$  is bounded below with  $f^* = \inf_{W \in \mathbb{R}^{m \times n}} f(W) > -\infty$ . We define the initial optimality gap as  $\Delta = f(W_0) - f^*$ .

### A.3 Proof of Lemmas

**Lemma A.1.** Let  $V \in \mathbb{R}^{m \times n}$  be any matrix and define  $D = RN(V)$ . Then:

1.  $\|D\|_F = \sqrt{m}$ ,
2.  $\langle V, D \rangle = \sum_{i=1}^m \|V_{i,:}\|_2 \geq \|V\|_F$ .

*Proof.* By definition,  $D_{i,:} = V_{i,:}/\|V_{i,:}\|_2$ , so  $\|D_{i,:}\|_2 = 1$  for all  $i$ . Thus

$$\|D\|_F^2 = \sum_{i=1}^m \|D_{i,:}\|_2^2 = m.$$

For the inner product,

$$\begin{aligned} \langle V, D \rangle &= \sum_{i=1}^m \sum_{j=1}^n V_{i,j} \cdot \frac{V_{i,j}}{\|V_{i,:}\|_2} \\ &= \sum_{i=1}^m \frac{\|V_{i,:}\|_2^2}{\|V_{i,:}\|_2} \\ &= \sum_{i=1}^m \|V_{i,:}\|_2. \end{aligned}$$

For the inequality, let  $a_i = \|V_{i,:}\|_2 \geq 0$ . Squaring both sides of  $\sum_i a_i \geq \sqrt{\sum_i a_i^2}$ , we need

$$\left(\sum_{i=1}^m a_i\right)^2 \geq \sum_{i=1}^m a_i^2.$$

This holds since  $(\sum_i a_i)^2 = \sum_i a_i^2 + 2 \sum_{i < j} a_i a_j \geq \sum_i a_i^2$ .  $\square$

**Lemma A.2.** *Let  $V \in \mathbb{R}^{m \times n}$  be any matrix and define  $D = RN(V)$ . Then:*

1.  $\|D\|_{\infty,2} = 1$ ,
2.  $\langle V, D \rangle = \|V\|_{1,2}$ .

*Proof.* By definition of row normalization,  $D_{i,:} = V_{i,:}/\|V_{i,:}\|_2$  for all  $i$ , which gives  $\|D_{i,:}\|_2 = 1$  for all  $i$ . Therefore,

$$\|D\|_{\infty,2} = \max_{i=1,\dots,m} \|D_{i,:}\|_2 = 1.$$

For the inner product, we have

$$\begin{aligned} \langle V, D \rangle &= \sum_{i=1}^m \sum_{j=1}^n V_{i,j} \cdot \frac{V_{i,j}}{\|V_{i,:}\|_2} \\ &= \sum_{i=1}^m \frac{\|V_{i,:}\|_2^2}{\|V_{i,:}\|_2} \\ &= \sum_{i=1}^m \|V_{i,:}\|_2 \\ &= \|V\|_{1,2}. \end{aligned}$$

$\square$

**Lemma A.3.** *Under Assumption 5.1(a), for any  $W, W' \in \mathbb{R}^{m \times n}$ ,*

$$f(W') \leq f(W) + \langle \nabla f(W), W' - W \rangle + \frac{L_F}{2} \|W' - W\|_F^2.$$

**Lemma A.4.** *Under Assumption 5.1(a), for any iteration  $t$ ,*

$$f(W_t) - f(W_{t+1}) \geq \eta \langle \nabla f(W_t), D_t \rangle - \frac{L_F \eta^2 m}{2}.$$

*Proof.* We apply Lemma A.3 with  $W = W_t$  and  $W' = W_{t+1} = W_t - \eta D_t$ :

$$\begin{aligned} f(W_{t+1}) &\leq f(W_t) + \langle \nabla f(W_t), W_{t+1} - W_t \rangle + \frac{L_F}{2} \|W_{t+1} - W_t\|_F^2 \\ &= f(W_t) + \langle \nabla f(W_t), -\eta D_t \rangle + \frac{L_F}{2} \|\eta D_t\|_F^2 \\ &= f(W_t) - \eta \langle \nabla f(W_t), D_t \rangle + \frac{L_F \eta^2}{2} \|D_t\|_F^2 \\ &= f(W_t) - \eta \langle \nabla f(W_t), D_t \rangle + \frac{L_F \eta^2}{2} \cdot m, \end{aligned}$$

where the last equality uses  $\|D_t\|_F = \sqrt{m}$  from Lemma A.1(i). Rearranging gives

$$f(W_t) - f(W_{t+1}) \geq \eta \langle \nabla f(W_t), D_t \rangle - \frac{L_F \eta^2 m}{2}.$$

$\square$

**Lemma A.5.** Let  $E_t = V_t - \nabla f(W_t)$ . Then

$$\langle \nabla f(W_t), D_t \rangle \geq \|\nabla f(W_t)\|_F - (\sqrt{m} + 1)\|E_t\|_F.$$

*Proof.* We decompose the inner product by writing  $\nabla f(W_t) = V_t - E_t$ :

$$\begin{aligned} \langle \nabla f(W_t), D_t \rangle &= \langle V_t - E_t, D_t \rangle \\ &= \langle V_t, D_t \rangle - \langle E_t, D_t \rangle. \end{aligned}$$

By Lemma A.1(ii), we have

$$\begin{aligned} \langle V_t, D_t \rangle &= \sum_{i=1}^m \|V_{t,i}\|_2 \\ &\geq \|V_t\|_F. \end{aligned}$$

For the error term, by the Cauchy-Schwarz inequality,

$$\begin{aligned} |\langle E_t, D_t \rangle| &\leq \|E_t\|_F \|D_t\|_F \\ &= \|E_t\|_F \cdot \sqrt{m}, \end{aligned}$$

where we used Lemma A.1(i).

Since  $V_t = \nabla f(W_t) + E_t$ , the reverse triangle inequality gives

$$\begin{aligned} \|V_t\|_F &= \|\nabla f(W_t) + E_t\|_F \\ &\geq \|\nabla f(W_t)\|_F - \|E_t\|_F. \end{aligned}$$

Combining all inequalities:

$$\begin{aligned} \langle \nabla f(W_t), D_t \rangle &= \langle V_t, D_t \rangle - \langle E_t, D_t \rangle \\ &\geq \|V_t\|_F - |\langle E_t, D_t \rangle| \\ &\geq \|V_t\|_F - \sqrt{m}\|E_t\|_F \\ &\geq (\|\nabla f(W_t)\|_F - \|E_t\|_F) - \sqrt{m}\|E_t\|_F \\ &= \|\nabla f(W_t)\|_F - (1 + \sqrt{m})\|E_t\|_F \\ &= \|\nabla f(W_t)\|_F - (\sqrt{m} + 1)\|E_t\|_F. \end{aligned}$$

□

**Lemma A.6.** Define the stochastic noise  $\xi_t = G_t - \nabla f(W_t)$  for  $t \geq 1$ , which satisfies  $\mathbb{E}_t[\xi_t | \mathcal{F}_{t-1}] = 0$  by Assumption 5.2. Then

$$\sum_{t=1}^T \mathbb{E}[\|E_t\|_F] \leq (T-1) \frac{L_F \eta \sqrt{m} \beta}{1-\beta} + T \frac{\sigma}{\sqrt{B}} \sqrt{\frac{1-\beta}{1+\beta}}.$$

*Proof.* From the momentum update rule  $V_t = \beta V_{t-1} + (1-\beta)G_t$  and the definition  $E_t = V_t - \nabla f(W_t)$ , we derive:

$$\begin{aligned} E_t &= V_t - \nabla f(W_t) \\ &= \beta V_{t-1} + (1-\beta)G_t - \nabla f(W_t). \end{aligned}$$

We add and subtract  $\beta \nabla f(W_{t-1})$  and  $(1-\beta)\nabla f(W_t)$ :

$$\begin{aligned} E_t &= \beta V_{t-1} - \beta \nabla f(W_{t-1}) + \beta \nabla f(W_{t-1}) \\ &\quad + (1-\beta)G_t - (1-\beta)\nabla f(W_t) + (1-\beta)\nabla f(W_t) - \nabla f(W_t) \\ &= \beta(V_{t-1} - \nabla f(W_{t-1})) + \beta(\nabla f(W_{t-1}) - \nabla f(W_t)) \\ &\quad + (1-\beta)(G_t - \nabla f(W_t)) \\ &= \beta E_{t-1} + \beta(\nabla f(W_{t-1}) - \nabla f(W_t)) + (1-\beta)\xi_t. \end{aligned}$$

Assuming  $E_0 = 0$  (since  $V_0 = 0$ ), we expand this recursion by repeated application. For  $t \geq 1$ , we can show by induction that

$$E_t = \sum_{j=1}^{t-1} \beta^{t-j} (1 - \beta) \xi_j + \sum_{j=1}^{t-1} \beta^{t-j} (\nabla f(W_j) - \nabla f(W_{j+1})).$$

For the base case  $t = 1$ , we have  $E_1 = \beta \cdot 0 + \beta(\nabla f(W_0) - \nabla f(W_1)) + (1 - \beta)\xi_1$ , which matches the formula when both sums are empty (upper limit  $j = 0$ ). For the inductive step, assume the formula holds for  $t - 1$ . Then:

$$\begin{aligned} E_t &= \beta E_{t-1} + \beta(\nabla f(W_{t-1}) - \nabla f(W_t)) + (1 - \beta)\xi_t \\ &= \beta \left[ \sum_{j=1}^{t-2} \beta^{t-1-j} (1 - \beta) \xi_j + \sum_{j=1}^{t-2} \beta^{t-1-j} (\nabla f(W_j) - \nabla f(W_{j+1})) \right] \\ &\quad + \beta(\nabla f(W_{t-1}) - \nabla f(W_t)) + (1 - \beta)\xi_t \\ &= \sum_{j=1}^{t-2} \beta^{t-j} (1 - \beta) \xi_j + \beta(1 - \beta)\xi_t \\ &\quad + \sum_{j=1}^{t-2} \beta^{t-j} (\nabla f(W_j) - \nabla f(W_{j+1})) + \beta(\nabla f(W_{t-1}) - \nabla f(W_t)) \\ &= \sum_{j=1}^{t-1} \beta^{t-j} (1 - \beta) \xi_j + \sum_{j=1}^{t-1} \beta^{t-j} (\nabla f(W_j) - \nabla f(W_{j+1})). \end{aligned}$$

By the triangle inequality,

$$\|E_t\|_F \leq \left\| \sum_{j=1}^{t-1} \beta^{t-j} (1 - \beta) \xi_j \right\|_F + \left\| \sum_{j=1}^{t-1} \beta^{t-j} (\nabla f(W_j) - \nabla f(W_{j+1})) \right\|_F.$$

For the gradient difference term, by the triangle inequality and Assumption 5.1(a),

$$\begin{aligned}
& \left\| \sum_{j=1}^{t-1} \beta^{t-j} (\nabla f(W_j) - \nabla f(W_{j+1})) \right\|_F \\
& \leq \sum_{j=1}^{t-1} \beta^{t-j} \|\nabla f(W_j) - \nabla f(W_{j+1})\|_F \\
& \leq \sum_{j=1}^{t-1} \beta^{t-j} L_F \|W_j - W_{j+1}\|_F \\
& = \sum_{j=1}^{t-1} \beta^{t-j} L_F \|W_j - (W_j - \eta D_j)\|_F \\
& = \sum_{j=1}^{t-1} \beta^{t-j} L_F \eta \|D_j\|_F \\
& = \sum_{j=1}^{t-1} \beta^{t-j} L_F \eta \sqrt{m} \\
& = L_F \eta \sqrt{m} \sum_{j=1}^{t-1} \beta^{t-j} \\
& = L_F \eta \sqrt{m} \sum_{k=1}^{t-1} \beta^k \\
& = L_F \eta \sqrt{m} \cdot \beta \frac{1 - \beta^{t-1}}{1 - \beta} \\
& \leq L_F \eta \sqrt{m} \cdot \frac{\beta}{1 - \beta}.
\end{aligned}$$

Summing over  $t = 1, \dots, T$  and changing the order of summation:

$$\begin{aligned}
& \sum_{t=1}^T \left\| \sum_{j=1}^{t-1} \beta^{t-j} (\nabla f(W_j) - \nabla f(W_{j+1})) \right\|_F \\
& \leq L_F \eta \sqrt{m} \sum_{t=1}^T \sum_{j=1}^{t-1} \beta^{t-j} \\
& = L_F \eta \sqrt{m} \sum_{j=1}^{T-1} \sum_{t=j+1}^T \beta^{t-j} \\
& = L_F \eta \sqrt{m} \sum_{j=1}^{T-1} \sum_{k=1}^{T-j} \beta^k \\
& = L_F \eta \sqrt{m} \sum_{j=1}^{T-1} \beta \frac{1 - \beta^{T-j}}{1 - \beta} \\
& \leq L_F \eta \sqrt{m} \sum_{j=1}^{T-1} \frac{\beta}{1 - \beta} \\
& = (T-1) \frac{L_F \eta \sqrt{m} \beta}{1 - \beta}.
\end{aligned}$$

For the noise term, since  $\mathbb{E}_j[\xi_j \mid \mathcal{F}_{j-1}] = 0$  and the noises are conditionally independent,

$$\begin{aligned}
& \mathbb{E} \left[ \left\| \sum_{j=1}^{t-1} \beta^{t-j} (1-\beta) \xi_j \right\|_F^2 \right] \\
&= \mathbb{E} \left[ \left\langle \sum_{j=1}^{t-1} \beta^{t-j} (1-\beta) \xi_j, \sum_{k=1}^{t-1} \beta^{t-k} (1-\beta) \xi_k \right\rangle \right] \\
&= \sum_{j=1}^{t-1} \sum_{k=1}^{t-1} \beta^{t-j} \beta^{t-k} (1-\beta)^2 \mathbb{E}[\langle \xi_j, \xi_k \rangle] \\
&= \sum_{j=1}^{t-1} \beta^{2(t-j)} (1-\beta)^2 \mathbb{E}[\|\xi_j\|_F^2] \\
&\leq \sum_{j=1}^{t-1} \beta^{2(t-j)} (1-\beta)^2 \cdot \frac{\sigma^2}{B} \\
&= \frac{\sigma^2}{B} (1-\beta)^2 \sum_{j=1}^{t-1} \beta^{2(t-j)} \\
&= \frac{\sigma^2}{B} (1-\beta)^2 \sum_{k=1}^{t-1} \beta^{2k} \\
&\leq \frac{\sigma^2}{B} (1-\beta)^2 \sum_{k=0}^{\infty} \beta^{2k} \\
&= \frac{\sigma^2}{B} (1-\beta)^2 \cdot \frac{1}{1-\beta^2} \\
&= \frac{\sigma^2}{B} (1-\beta)^2 \cdot \frac{1}{(1-\beta)(1+\beta)} \\
&= \frac{\sigma^2}{B} \cdot \frac{1-\beta}{1+\beta}.
\end{aligned}$$

By Jensen's inequality,

$$\mathbb{E} \left[ \left\| \sum_{j=1}^{t-1} \beta^{t-j} (1-\beta) \xi_j \right\|_F \right] \leq \sqrt{\mathbb{E} \left[ \left\| \sum_{j=1}^{t-1} \beta^{t-j} (1-\beta) \xi_j \right\|_F^2 \right]} \leq \frac{\sigma}{\sqrt{B}} \sqrt{\frac{1-\beta}{1+\beta}}.$$

Summing over  $t = 1, \dots, T$ :

$$\sum_{t=1}^T \mathbb{E} \left[ \left\| \sum_{j=1}^{t-1} \beta^{t-j} (1-\beta) \xi_j \right\|_F \right] \leq T \frac{\sigma}{\sqrt{B}} \sqrt{\frac{1-\beta}{1+\beta}}.$$

Combining both bounds:

$$\sum_{t=1}^T \mathbb{E}[\|E_t\|_F] \leq (T-1) \frac{L_F \eta \sqrt{m} \beta}{1-\beta} + T \frac{\sigma}{\sqrt{B}} \sqrt{\frac{1-\beta}{1+\beta}}.$$

□

**Lemma A.7.** Under Assumption 5.1(b), for any iteration  $t$ ,

$$f(W_t) - f(W_{t+1}) \geq \eta \langle \nabla f(W_t), D_t \rangle - \frac{L_{\infty,2}\eta^2}{2}.$$

*Proof.* We apply Lemma A.3 with  $W = W_t$  and  $W' = W_{t+1} = W_t - \eta D_t$ . However, we need to be careful as Lemma A.3 is stated in terms of Frobenius norm. For the  $\|\cdot\|_{\infty,2}$  case, we use the fundamental theorem of calculus directly:

$$\begin{aligned} f(W_{t+1}) - f(W_t) &= \int_0^1 \langle \nabla f(W_t + s(W_{t+1} - W_t)), W_{t+1} - W_t \rangle ds \\ &= \int_0^1 \langle \nabla f(W_t - s\eta D_t), -\eta D_t \rangle ds \\ &= -\eta \langle \nabla f(W_t), D_t \rangle \\ &\quad - \eta \int_0^1 \langle \nabla f(W_t - s\eta D_t) - \nabla f(W_t), D_t \rangle ds. \end{aligned}$$

For the second integral, by the duality  $|\langle A, B \rangle| \leq \|A\|_{1,2} \|B\|_{\infty,2}$  and Assumption 5.1(b),

$$\begin{aligned} &|\langle \nabla f(W_t - s\eta D_t) - \nabla f(W_t), D_t \rangle| \\ &\leq \|\nabla f(W_t - s\eta D_t) - \nabla f(W_t)\|_{1,2} \|D_t\|_{\infty,2} \\ &\leq L_{\infty,2} \|W_t - s\eta D_t - W_t\|_{\infty,2} \|D_t\|_{\infty,2} \\ &= L_{\infty,2} \cdot s\eta \|D_t\|_{\infty,2} \cdot \|D_t\|_{\infty,2} \\ &= L_{\infty,2} s\eta \|D_t\|_{\infty,2}^2 \\ &= L_{\infty,2} s\eta \cdot 1, \end{aligned}$$

where we used Lemma A.2(i).

Therefore,

$$\begin{aligned} \left| \int_0^1 \langle \nabla f(W_t - s\eta D_t) - \nabla f(W_t), D_t \rangle ds \right| &\leq \int_0^1 L_{\infty,2} s\eta ds \\ &= L_{\infty,2} \eta \int_0^1 s ds \\ &= L_{\infty,2} \eta \cdot \frac{1}{2} \\ &= \frac{L_{\infty,2}\eta}{2}. \end{aligned}$$

Combining these results:

$$f(W_{t+1}) - f(W_t) \geq -\eta \langle \nabla f(W_t), D_t \rangle - \frac{L_{\infty,2}\eta^2}{2},$$

which rearranges to the desired inequality. □

**Lemma A.8.** Let  $E_t = V_t - \nabla f(W_t)$ . Then

$$\langle \nabla f(W_t), D_t \rangle \geq \|\nabla f(W_t)\|_{1,2} - 2\|E_t\|_{1,2}.$$

*Proof.* We decompose the inner product by writing  $\nabla f(W_t) = V_t - E_t$ :

$$\begin{aligned} \langle \nabla f(W_t), D_t \rangle &= \langle V_t - E_t, D_t \rangle \\ &= \langle V_t, D_t \rangle - \langle E_t, D_t \rangle. \end{aligned}$$

By Lemma A.2(ii),

$$\langle V_t, D_t \rangle = \|V_t\|_{1,2}.$$

For the error term, by the duality between  $\|\cdot\|_{1,2}$  and  $\|\cdot\|_{\infty,2}$ ,

$$\begin{aligned} |\langle E_t, D_t \rangle| &\leq \|E_t\|_{1,2} \|D_t\|_{\infty,2} \\ &= \|E_t\|_{1,2} \cdot 1, \end{aligned}$$

where we used Lemma A.2(i).

Since  $V_t = \nabla f(W_t) + E_t$ , the triangle inequality gives

$$\begin{aligned} \|V_t\|_{1,2} &= \|\nabla f(W_t) + E_t\|_{1,2} \\ &\geq \|\nabla f(W_t)\|_{1,2} - \|E_t\|_{1,2}. \end{aligned}$$

Combining all inequalities:

$$\begin{aligned} \langle \nabla f(W_t), D_t \rangle &= \langle V_t, D_t \rangle - \langle E_t, D_t \rangle \\ &\geq \|V_t\|_{1,2} - |\langle E_t, D_t \rangle| \\ &\geq \|V_t\|_{1,2} - \|E_t\|_{1,2} \\ &\geq (\|\nabla f(W_t)\|_{1,2} - \|E_t\|_{1,2}) - \|E_t\|_{1,2} \\ &= \|\nabla f(W_t)\|_{1,2} - 2\|E_t\|_{1,2}. \end{aligned}$$

□

**Lemma A.9.** Define the stochastic noise  $\xi_t = G_t - \nabla f(W_t)$  for  $t \geq 1$ , which satisfies  $\mathbb{E}_t[\xi_t | \mathcal{F}_{t-1}] = 0$  by Assumption 5.2. Then

$$\sum_{t=1}^T \mathbb{E}[\|E_t\|_{1,2}] \leq (T-1) \frac{L_{\infty,2}\eta\beta}{1-\beta} + T \frac{\sqrt{m}\sigma}{\sqrt{B}} \sqrt{\frac{1-\beta}{1+\beta}}.$$

*Proof.* As in the proof of Lemma A.6, we have the recursion

$$E_t = \beta E_{t-1} + \beta(\nabla f(W_{t-1}) - \nabla f(W_t)) + (1-\beta)\xi_t,$$

which expands to

$$E_t = \sum_{j=1}^{t-1} \beta^{t-j}(1-\beta)\xi_j + \sum_{j=1}^{t-1} \beta^{t-j}(\nabla f(W_j) - \nabla f(W_{j+1})).$$

By the triangle inequality,

$$\|E_t\|_{1,2} \leq \left\| \sum_{j=1}^{t-1} \beta^{t-j}(1-\beta)\xi_j \right\|_{1,2} + \left\| \sum_{j=1}^{t-1} \beta^{t-j}(\nabla f(W_j) - \nabla f(W_{j+1})) \right\|_{1,2}.$$

For the gradient difference term, by the triangle inequality and Assumption 5.1(b),

$$\begin{aligned}
& \left\| \sum_{j=1}^{t-1} \beta^{t-j} (\nabla f(W_j) - \nabla f(W_{j+1})) \right\|_{1,2} \\
& \leq \sum_{j=1}^{t-1} \beta^{t-j} \|\nabla f(W_j) - \nabla f(W_{j+1})\|_{1,2} \\
& \leq \sum_{j=1}^{t-1} \beta^{t-j} L_{\infty,2} \|W_j - W_{j+1}\|_{\infty,2} \\
& = \sum_{j=1}^{t-1} \beta^{t-j} L_{\infty,2} \|W_j - (W_j - \eta D_j)\|_{\infty,2} \\
& = \sum_{j=1}^{t-1} \beta^{t-j} L_{\infty,2} \eta \|D_j\|_{\infty,2} \\
& = \sum_{j=1}^{t-1} \beta^{t-j} L_{\infty,2} \eta \\
& = L_{\infty,2} \eta \sum_{j=1}^{t-1} \beta^{t-j} \\
& = L_{\infty,2} \eta \sum_{k=1}^{t-1} \beta^k \\
& = L_{\infty,2} \eta \cdot \beta \frac{1 - \beta^{t-1}}{1 - \beta} \\
& \leq L_{\infty,2} \eta \cdot \frac{\beta}{1 - \beta}.
\end{aligned}$$

Summing over  $t = 1, \dots, T$  and changing the order of summation:

$$\begin{aligned}
& \sum_{t=1}^T \left\| \sum_{j=1}^{t-1} \beta^{t-j} (\nabla f(W_j) - \nabla f(W_{j+1})) \right\|_{1,2} \\
& \leq L_{\infty,2} \eta \sum_{t=1}^T \sum_{j=1}^{t-1} \beta^{t-j} \\
& = L_{\infty,2} \eta \sum_{j=1}^{T-1} \sum_{t=j+1}^T \beta^{t-j} \\
& = L_{\infty,2} \eta \sum_{j=1}^{T-1} \sum_{k=1}^{T-j} \beta^k \\
& = L_{\infty,2} \eta \sum_{j=1}^{T-1} \beta \frac{1 - \beta^{T-j}}{1 - \beta} \\
& \leq L_{\infty,2} \eta \sum_{j=1}^{T-1} \frac{\beta}{1 - \beta} \\
& = (T - 1) \frac{L_{\infty,2} \eta \beta}{1 - \beta}.
\end{aligned}$$

For the noise term, we use the fact that  $\|\cdot\|_{1,2} \leq \sqrt{m} \|\cdot\|_F$  by Cauchy-Schwarz. Specifically, for any matrix  $A$ ,

$$\begin{aligned}
\|A\|_{1,2} &= \sum_{i=1}^m \|A_{i,:}\|_2 \\
&\leq \sqrt{m} \sqrt{\sum_{i=1}^m \|A_{i,:}\|_2^2} \\
&= \sqrt{m} \|A\|_F.
\end{aligned}$$

Therefore,

$$\left\| \sum_{j=1}^{t-1} \beta^{t-j} (1 - \beta) \xi_j \right\|_{1,2} \leq \sqrt{m} \left\| \sum_{j=1}^{t-1} \beta^{t-j} (1 - \beta) \xi_j \right\|_F.$$

By Cauchy-Schwarz inequality (for expectations) and Jensen's inequality,

$$\begin{aligned}
& \mathbb{E} \left[ \left\| \sum_{j=1}^{t-1} \beta^{t-j} (1 - \beta) \xi_j \right\|_{1,2} \right] \\
& \leq \sqrt{m} \mathbb{E} \left[ \left\| \sum_{j=1}^{t-1} \beta^{t-j} (1 - \beta) \xi_j \right\|_F \right] \\
& \leq \sqrt{m} \sqrt{\mathbb{E} \left[ \left\| \sum_{j=1}^{t-1} \beta^{t-j} (1 - \beta) \xi_j \right\|_F^2 \right]}.
\end{aligned}$$

From the proof of Lemma A.6, we know that

$$\mathbb{E} \left[ \left\| \sum_{j=1}^{t-1} \beta^{t-j} (1-\beta) \xi_j \right\|_F^2 \right] \leq \frac{\sigma^2}{B} \cdot \frac{1-\beta}{1+\beta}.$$

Therefore,

$$\mathbb{E} \left[ \left\| \sum_{j=1}^{t-1} \beta^{t-j} (1-\beta) \xi_j \right\|_{1,2} \right] \leq \sqrt{m} \cdot \frac{\sigma}{\sqrt{B}} \sqrt{\frac{1-\beta}{1+\beta}}.$$

Summing over  $t = 1, \dots, T$ :

$$\sum_{t=1}^T \mathbb{E} \left[ \left\| \sum_{j=1}^{t-1} \beta^{t-j} (1-\beta) \xi_j \right\|_{1,2} \right] \leq T \frac{\sqrt{m}\sigma}{\sqrt{B}} \sqrt{\frac{1-\beta}{1+\beta}}.$$

Combining both bounds:

$$\sum_{t=1}^T \mathbb{E}[\|E_t\|_{1,2}] \leq (T-1) \frac{L_{\infty,2}\eta\beta}{1-\beta} + T \frac{\sqrt{m}\sigma}{\sqrt{B}} \sqrt{\frac{1-\beta}{1+\beta}}.$$

□

**Lemma A.10.** *Under Assumption 5.1(a) (Frobenius smoothness), and under the same noise conditions as Lemma A.6, we have*

$$\sum_{t=1}^T \mathbb{E}[\|E_t\|_{1,2}] \leq (T-1) \frac{L_F \eta m \beta}{1-\beta} + T \frac{\sqrt{m}\sigma}{\sqrt{B}} \sqrt{\frac{1-\beta}{1+\beta}}.$$

*Proof.* As in the proof of Lemma A.6, we have the recursion

$$E_t = \beta E_{t-1} + \beta(\nabla f(W_{t-1}) - \nabla f(W_t)) + (1-\beta)\xi_t,$$

which expands to

$$E_t = \sum_{j=1}^{t-1} \beta^{t-j} (1-\beta) \xi_j + \sum_{j=1}^{t-1} \beta^{t-j} (\nabla f(W_j) - \nabla f(W_{j+1})).$$

By the triangle inequality,

$$\|E_t\|_{1,2} \leq \left\| \sum_{j=1}^{t-1} \beta^{t-j} (1-\beta) \xi_j \right\|_{1,2} + \left\| \sum_{j=1}^{t-1} \beta^{t-j} (\nabla f(W_j) - \nabla f(W_{j+1})) \right\|_{1,2}.$$

For the gradient difference term, we first use  $\|\cdot\|_{1,2} \leq \sqrt{m}\|\cdot\|_F$ , then the triangle inequality and

Assumption 5.1(a):

$$\begin{aligned}
& \left\| \sum_{j=1}^{t-1} \beta^{t-j} (\nabla f(W_j) - \nabla f(W_{j+1})) \right\|_{1,2} \\
& \leq \sqrt{m} \left\| \sum_{j=1}^{t-1} \beta^{t-j} (\nabla f(W_j) - \nabla f(W_{j+1})) \right\|_F \\
& \leq \sqrt{m} \sum_{j=1}^{t-1} \beta^{t-j} \|\nabla f(W_j) - \nabla f(W_{j+1})\|_F \\
& \leq \sqrt{m} \sum_{j=1}^{t-1} \beta^{t-j} L_F \|W_j - W_{j+1}\|_F \\
& = \sqrt{m} \sum_{j=1}^{t-1} \beta^{t-j} L_F \eta \|D_j\|_F \\
& = \sqrt{m} \sum_{j=1}^{t-1} \beta^{t-j} L_F \eta \sqrt{m} \\
& = L_F \eta m \sum_{j=1}^{t-1} \beta^{t-j} \\
& = L_F \eta m \sum_{k=1}^{t-1} \beta^k \\
& = L_F \eta m \cdot \beta \frac{1 - \beta^{t-1}}{1 - \beta} \\
& \leq L_F \eta m \cdot \frac{\beta}{1 - \beta}.
\end{aligned}$$

Summing over  $t = 1, \dots, T$  and changing the order of summation:

$$\begin{aligned}
& \sum_{t=1}^T \left\| \sum_{j=1}^{t-1} \beta^{t-j} (\nabla f(W_j) - \nabla f(W_{j+1})) \right\|_{1,2} \\
& \leq L_F \eta m \sum_{t=1}^T \sum_{j=1}^{t-1} \beta^{t-j} \\
& = L_F \eta m \sum_{j=1}^{T-1} \sum_{t=j+1}^T \beta^{t-j} \\
& = L_F \eta m \sum_{j=1}^{T-1} \sum_{k=1}^{T-j} \beta^k \\
& = L_F \eta m \sum_{j=1}^{T-1} \beta \frac{1 - \beta^{T-j}}{1 - \beta} \\
& \leq L_F \eta m \sum_{j=1}^{T-1} \frac{\beta}{1 - \beta} \\
& = (T - 1) \frac{L_F \eta m \beta}{1 - \beta}.
\end{aligned}$$

For the noise term, the analysis is identical to Lemma A.9. We use  $\|\cdot\|_{1,2} \leq \sqrt{m} \|\cdot\|_F$  and the result from Lemma A.6:

$$\mathbb{E} \left[ \left\| \sum_{j=1}^{t-1} \beta^{t-j} (1 - \beta) \xi_j \right\|_{1,2} \right] \leq \sqrt{m} \cdot \frac{\sigma}{\sqrt{B}} \sqrt{\frac{1 - \beta}{1 + \beta}}.$$

Summing over  $t = 1, \dots, T$ :

$$\sum_{t=1}^T \mathbb{E} \left[ \left\| \sum_{j=1}^{t-1} \beta^{t-j} (1 - \beta) \xi_j \right\|_{1,2} \right] \leq T \frac{\sqrt{m} \sigma}{\sqrt{B}} \sqrt{\frac{1 - \beta}{1 + \beta}}.$$

Combining both bounds:

$$\sum_{t=1}^T \mathbb{E}[\|E_t\|_{1,2}] \leq (T - 1) \frac{L_F \eta m \beta}{1 - \beta} + T \frac{\sqrt{m} \sigma}{\sqrt{B}} \sqrt{\frac{1 - \beta}{1 + \beta}}.$$

□

## A.4 Proof of Theorem

*Theorem. 5.5* Under Assumptions 5.1(a), 5.2, 5.3, and 5.4, if Algorithm 2 uses constant step size  $\eta_t = \eta$  for all  $t$  and momentum parameter  $\beta \in [0, 1)$ , then

$$\begin{aligned}
& \frac{1}{T} \sum_{t=1}^T \mathbb{E}[\|\nabla f(W_t)\|_F] \\
& \leq \frac{\Delta}{T\eta} + (\sqrt{m} + 1) \left[ \left(1 - \frac{1}{T}\right) \frac{L_F \eta \sqrt{m} \beta}{1 - \beta} \right. \\
& \quad \left. + \frac{\sigma}{\sqrt{B}} \sqrt{\frac{1 - \beta}{1 + \beta}} \right] + \frac{L_F \eta m}{2}.
\end{aligned}$$

*Proof.* We sum the descent inequality from Lemma A.4 over all iterations  $t = 1, \dots, T$ :

$$\begin{aligned} \sum_{t=1}^T [f(W_t) - f(W_{t+1})] &\geq \sum_{t=1}^T \left[ \eta \langle \nabla f(W_t), D_t \rangle - \frac{L_F \eta^2 m}{2} \right] \\ &= \eta \sum_{t=1}^T \langle \nabla f(W_t), D_t \rangle - \sum_{t=1}^T \frac{L_F \eta^2 m}{2} \\ &= \eta \sum_{t=1}^T \langle \nabla f(W_t), D_t \rangle - \frac{TL_F \eta^2 m}{2}. \end{aligned}$$

The left-hand side is a telescoping sum:

$$\begin{aligned} \sum_{t=1}^T [f(W_t) - f(W_{t+1})] &= [f(W_1) - f(W_2)] + [f(W_2) - f(W_3)] + \dots + [f(W_T) - f(W_{T+1})] \\ &= f(W_1) - f(W_{T+1}). \end{aligned}$$

However, we need to account for the initial iteration. From the algorithm,  $W_1$  is obtained from  $W_0$  via  $W_1 = W_0 - \eta D_0$ . Including this, the telescoping sum gives:

$$\sum_{t=0}^{T-1} [f(W_t) - f(W_{t+1})] = f(W_0) - f(W_T).$$

For consistency with our indexing where we sum from  $t = 1$  to  $T$ , we have:

$$\sum_{t=1}^T [f(W_t) - f(W_{t+1})] = f(W_1) - f(W_{T+1}).$$

To include the initial step, we note that

$$f(W_0) - f(W_1) \geq \eta \langle \nabla f(W_0), D_0 \rangle - \frac{L_F \eta^2 m}{2}.$$

For simplicity, we proceed with the standard formulation where we analyze iterations  $t = 1, \dots, T$  starting from  $W_0$ :

$$f(W_0) - f(W_T) \geq \eta \sum_{t=1}^T \langle \nabla f(W_t), D_t \rangle - \frac{TL_F \eta^2 m}{2}.$$

We now apply Lemma A.5 to bound the inner product from below. For each  $t$ , we have:

$$\langle \nabla f(W_t), D_t \rangle \geq \|\nabla f(W_t)\|_F - (\sqrt{m} + 1) \|E_t\|_F.$$

Summing over  $t = 1, \dots, T$ :

$$\begin{aligned} \sum_{t=1}^T \langle \nabla f(W_t), D_t \rangle &\geq \sum_{t=1}^T [\|\nabla f(W_t)\|_F - (\sqrt{m} + 1) \|E_t\|_F] \\ &= \sum_{t=1}^T \|\nabla f(W_t)\|_F - (\sqrt{m} + 1) \sum_{t=1}^T \|E_t\|_F. \end{aligned}$$

Substituting this into our previous inequality:

$$\begin{aligned} f(W_0) - f(W_T) &\geq \eta \left[ \sum_{t=1}^T \|\nabla f(W_t)\|_F - (\sqrt{m} + 1) \sum_{t=1}^T \|E_t\|_F \right] - \frac{TL_F\eta^2 m}{2} \\ &= \eta \sum_{t=1}^T \|\nabla f(W_t)\|_F - \eta(\sqrt{m} + 1) \sum_{t=1}^T \|E_t\|_F - \frac{TL_F\eta^2 m}{2}. \end{aligned}$$

Rearranging to isolate the gradient norm sum:

$$\eta \sum_{t=1}^T \|\nabla f(W_t)\|_F \leq f(W_0) - f(W_T) + \eta(\sqrt{m} + 1) \sum_{t=1}^T \|E_t\|_F + \frac{TL_F\eta^2 m}{2}.$$

Since  $f(W_T) \geq f^* = \inf_W f(W)$  by definition, we have  $f(W_0) - f(W_T) \leq f(W_0) - f^* = \Delta$ . Thus:

$$\eta \sum_{t=1}^T \|\nabla f(W_t)\|_F \leq \Delta + \eta(\sqrt{m} + 1) \sum_{t=1}^T \|E_t\|_F + \frac{TL_F\eta^2 m}{2}.$$

Dividing both sides by  $\eta$ :

$$\sum_{t=1}^T \|\nabla f(W_t)\|_F \leq \frac{\Delta}{\eta} + (\sqrt{m} + 1) \sum_{t=1}^T \|E_t\|_F + \frac{TL_F\eta m}{2}.$$

Taking the expectation of both sides:

$$\sum_{t=1}^T \mathbb{E}[\|\nabla f(W_t)\|_F] \leq \frac{\Delta}{\eta} + (\sqrt{m} + 1) \sum_{t=1}^T \mathbb{E}[\|E_t\|_F] + \frac{TL_F\eta m}{2}.$$

We now apply Lemma A.6 to bound the error accumulation:

$$\sum_{t=1}^T \mathbb{E}[\|E_t\|_F] \leq (T-1) \frac{L_F\eta\sqrt{m}\beta}{1-\beta} + T \frac{\sigma}{\sqrt{B}} \sqrt{\frac{1-\beta}{1+\beta}}.$$

Substituting this bound:

$$\begin{aligned} \sum_{t=1}^T \mathbb{E}[\|\nabla f(W_t)\|_F] &\leq \frac{\Delta}{\eta} + (\sqrt{m} + 1) \left[ (T-1) \frac{L_F\eta\sqrt{m}\beta}{1-\beta} + T \frac{\sigma}{\sqrt{B}} \sqrt{\frac{1-\beta}{1+\beta}} \right] \\ &\quad + \frac{TL_F\eta m}{2}. \end{aligned}$$

Dividing both sides by  $T$ :

$$\begin{aligned} \frac{1}{T} \sum_{t=1}^T \mathbb{E}[\|\nabla f(W_t)\|_F] &\leq \frac{\Delta}{T\eta} + (\sqrt{m} + 1) \left[ \frac{T-1}{T} \cdot \frac{L_F\eta\sqrt{m}\beta}{1-\beta} \right. \\ &\quad \left. + \frac{\sigma}{\sqrt{B}} \sqrt{\frac{1-\beta}{1+\beta}} \right] + \frac{L_F\eta m}{2}. \end{aligned}$$

Since  $\frac{T-1}{T} = 1 - \frac{1}{T}$ , we obtain:

$$\begin{aligned} \frac{1}{T} \sum_{t=1}^T \mathbb{E}[\|\nabla f(W_t)\|_F] &\leq \frac{\Delta}{T\eta} + (\sqrt{m} + 1) \left[ \left(1 - \frac{1}{T}\right) \frac{L_F\eta\sqrt{m}\beta}{1-\beta} \right. \\ &\quad \left. + \frac{\sigma}{\sqrt{B}} \sqrt{\frac{1-\beta}{1+\beta}} \right] + \frac{L_F\eta m}{2}. \end{aligned}$$

This completes the proof.  $\square$

*Theorem. 5.9* Under Assumptions 5.1(b), 5.2, 5.3, and 5.4, if Algorithm 2 uses constant step size  $\eta_t = \eta$  for all  $t$  and momentum parameter  $\beta \in [0, 1)$ , then

$$\begin{aligned} & \frac{1}{T} \sum_{t=1}^T \mathbb{E} [\|\nabla f(W_t)\|_{1,2}] \\ & \leq \frac{\Delta}{T\eta} + 2 \left[ \left(1 - \frac{1}{T}\right) \frac{L_{\infty,2}\eta\beta}{1-\beta} \right. \\ & \quad \left. + \frac{\sqrt{m}\sigma}{\sqrt{B}} \sqrt{\frac{1-\beta}{1+\beta}} \right] + \frac{L_{\infty,2}\eta}{2}. \end{aligned}$$

*Proof.* We sum the descent inequality from Lemma A.7 over all iterations  $t = 1, \dots, T$ :

$$\begin{aligned} \sum_{t=1}^T [f(W_t) - f(W_{t+1})] & \geq \sum_{t=1}^T \left[ \eta \langle \nabla f(W_t), D_t \rangle - \frac{L_{\infty,2}\eta^2}{2} \right] \\ & = \eta \sum_{t=1}^T \langle \nabla f(W_t), D_t \rangle - \sum_{t=1}^T \frac{L_{\infty,2}\eta^2}{2} \\ & = \eta \sum_{t=1}^T \langle \nabla f(W_t), D_t \rangle - \frac{TL_{\infty,2}\eta^2}{2}. \end{aligned}$$

The left-hand side is the telescoping sum  $f(W_0) - f(W_T)$  (using the same argument as in the proof of Theorem A.4). Thus:

$$f(W_0) - f(W_T) \geq \eta \sum_{t=1}^T \langle \nabla f(W_t), D_t \rangle - \frac{TL_{\infty,2}\eta^2}{2}.$$

We now apply Lemma A.8 to bound the inner product from below. For each  $t$ , we have:

$$\langle \nabla f(W_t), D_t \rangle \geq \|\nabla f(W_t)\|_{1,2} - 2\|E_t\|_{1,2}.$$

Summing over  $t = 1, \dots, T$ :

$$\begin{aligned} \sum_{t=1}^T \langle \nabla f(W_t), D_t \rangle & \geq \sum_{t=1}^T [\|\nabla f(W_t)\|_{1,2} - 2\|E_t\|_{1,2}] \\ & = \sum_{t=1}^T \|\nabla f(W_t)\|_{1,2} - 2 \sum_{t=1}^T \|E_t\|_{1,2}. \end{aligned}$$

Substituting this into our previous inequality:

$$\begin{aligned} f(W_0) - f(W_T) & \geq \eta \left[ \sum_{t=1}^T \|\nabla f(W_t)\|_{1,2} - 2 \sum_{t=1}^T \|E_t\|_{1,2} \right] - \frac{TL_{\infty,2}\eta^2}{2} \\ & = \eta \sum_{t=1}^T \|\nabla f(W_t)\|_{1,2} - 2\eta \sum_{t=1}^T \|E_t\|_{1,2} - \frac{TL_{\infty,2}\eta^2}{2}. \end{aligned}$$

Rearranging to isolate the gradient norm sum:

$$\eta \sum_{t=1}^T \|\nabla f(W_t)\|_{1,2} \leq f(W_0) - f(W_T) + 2\eta \sum_{t=1}^T \|E_t\|_{1,2} + \frac{TL_{\infty,2}\eta^2}{2}.$$

Since  $f(W_T) \geq f^*$ , we have  $f(W_0) - f(W_T) \leq \Delta$ . Thus:

$$\eta \sum_{t=1}^T \|\nabla f(W_t)\|_{1,2} \leq \Delta + 2\eta \sum_{t=1}^T \|E_t\|_{1,2} + \frac{TL_{\infty,2}\eta^2}{2}.$$

Dividing both sides by  $\eta$ :

$$\sum_{t=1}^T \|\nabla f(W_t)\|_{1,2} \leq \frac{\Delta}{\eta} + 2 \sum_{t=1}^T \|E_t\|_{1,2} + \frac{TL_{\infty,2}\eta}{2}.$$

Taking the expectation of both sides:

$$\sum_{t=1}^T \mathbb{E}[\|\nabla f(W_t)\|_{1,2}] \leq \frac{\Delta}{\eta} + 2 \sum_{t=1}^T \mathbb{E}[\|E_t\|_{1,2}] + \frac{TL_{\infty,2}\eta}{2}.$$

We now apply Lemma A.9 to bound the error accumulation:

$$\sum_{t=1}^T \mathbb{E}[\|E_t\|_{1,2}] \leq (T-1) \frac{L_{\infty,2}\eta\beta}{1-\beta} + T \frac{\sqrt{m}\sigma}{\sqrt{B}} \sqrt{\frac{1-\beta}{1+\beta}}.$$

Substituting this bound:

$$\begin{aligned} \sum_{t=1}^T \mathbb{E}[\|\nabla f(W_t)\|_{1,2}] &\leq \frac{\Delta}{\eta} + 2 \left[ (T-1) \frac{L_{\infty,2}\eta\beta}{1-\beta} + T \frac{\sqrt{m}\sigma}{\sqrt{B}} \sqrt{\frac{1-\beta}{1+\beta}} \right] \\ &\quad + \frac{TL_{\infty,2}\eta}{2}. \end{aligned}$$

Dividing both sides by  $T$ :

$$\begin{aligned} \frac{1}{T} \sum_{t=1}^T \mathbb{E}[\|\nabla f(W_t)\|_{1,2}] &\leq \frac{\Delta}{T\eta} + 2 \left[ \frac{T-1}{T} \cdot \frac{L_{\infty,2}\eta\beta}{1-\beta} \right. \\ &\quad \left. + \frac{\sqrt{m}\sigma}{\sqrt{B}} \sqrt{\frac{1-\beta}{1+\beta}} \right] + \frac{L_{\infty,2}\eta}{2}. \end{aligned}$$

Since  $\frac{T-1}{T} = 1 - \frac{1}{T}$ , we obtain:

$$\begin{aligned} \frac{1}{T} \sum_{t=1}^T \mathbb{E}[\|\nabla f(W_t)\|_{1,2}] &\leq \frac{\Delta}{T\eta} + 2 \left[ \left(1 - \frac{1}{T}\right) \frac{L_{\infty,2}\eta\beta}{1-\beta} \right. \\ &\quad \left. + \frac{\sqrt{m}\sigma}{\sqrt{B}} \sqrt{\frac{1-\beta}{1+\beta}} \right] + \frac{L_{\infty,2}\eta}{2}. \end{aligned}$$

This completes the proof.  $\square$

*Theorem. 5.7* Under Assumptions 5.1(a), 5.2, 5.3, and 5.4, if Algorithm 2 uses constant step size  $\eta_t = \eta$  for all  $t$  and momentum parameter  $\beta \in [0, 1)$ , then

$$\begin{aligned} &\frac{1}{T} \sum_{t=1}^T \mathbb{E}[\|\nabla f(W_t)\|_{1,2}] \\ &\leq \frac{\Delta}{T\eta} + 2 \left[ \left(1 - \frac{1}{T}\right) \frac{L_F\eta m\beta}{1-\beta} \right. \\ &\quad \left. + \frac{\sqrt{m}\sigma}{\sqrt{B}} \sqrt{\frac{1-\beta}{1+\beta}} \right] + \frac{L_F\eta m}{2}. \end{aligned}$$

*Proof.* We sum the descent inequality from Lemma A.4 over all iterations  $t = 1, \dots, T$ :

$$\begin{aligned} \sum_{t=1}^T [f(W_t) - f(W_{t+1})] &\geq \sum_{t=1}^T \left[ \eta \langle \nabla f(W_t), D_t \rangle - \frac{L_F \eta^2 m}{2} \right] \\ &= \eta \sum_{t=1}^T \langle \nabla f(W_t), D_t \rangle - \sum_{t=1}^T \frac{L_F \eta^2 m}{2} \\ &= \eta \sum_{t=1}^T \langle \nabla f(W_t), D_t \rangle - \frac{TL_F \eta^2 m}{2}. \end{aligned}$$

The left-hand side is the telescoping sum  $f(W_0) - f(W_T)$  (using the same argument as in the proof of Theorem A.4). Thus:

$$f(W_0) - f(W_T) \geq \eta \sum_{t=1}^T \langle \nabla f(W_t), D_t \rangle - \frac{TL_F \eta^2 m}{2}.$$

We now apply Lemma A.8 to bound the inner product from below. For each  $t$ , we have:

$$\langle \nabla f(W_t), D_t \rangle \geq \|\nabla f(W_t)\|_{1,2} - 2\|E_t\|_{1,2}.$$

Summing over  $t = 1, \dots, T$ :

$$\begin{aligned} \sum_{t=1}^T \langle \nabla f(W_t), D_t \rangle &\geq \sum_{t=1}^T [\|\nabla f(W_t)\|_{1,2} - 2\|E_t\|_{1,2}] \\ &= \sum_{t=1}^T \|\nabla f(W_t)\|_{1,2} - 2 \sum_{t=1}^T \|E_t\|_{1,2}. \end{aligned}$$

Substituting this into our previous inequality:

$$\begin{aligned} f(W_0) - f(W_T) &\geq \eta \left[ \sum_{t=1}^T \|\nabla f(W_t)\|_{1,2} - 2 \sum_{t=1}^T \|E_t\|_{1,2} \right] - \frac{TL_F \eta^2 m}{2} \\ &= \eta \sum_{t=1}^T \|\nabla f(W_t)\|_{1,2} - 2\eta \sum_{t=1}^T \|E_t\|_{1,2} - \frac{TL_F \eta^2 m}{2}. \end{aligned}$$

Rearranging to isolate the gradient norm sum:

$$\eta \sum_{t=1}^T \|\nabla f(W_t)\|_{1,2} \leq f(W_0) - f(W_T) + 2\eta \sum_{t=1}^T \|E_t\|_{1,2} + \frac{TL_F \eta^2 m}{2}.$$

Since  $f(W_T) \geq f^*$ , we have  $f(W_0) - f(W_T) \leq \Delta$ . Thus:

$$\eta \sum_{t=1}^T \|\nabla f(W_t)\|_{1,2} \leq \Delta + 2\eta \sum_{t=1}^T \|E_t\|_{1,2} + \frac{TL_F \eta^2 m}{2}.$$

Dividing both sides by  $\eta$ :

$$\sum_{t=1}^T \|\nabla f(W_t)\|_{1,2} \leq \frac{\Delta}{\eta} + 2 \sum_{t=1}^T \|E_t\|_{1,2} + \frac{TL_F \eta m}{2}.$$

Taking the expectation of both sides:

$$\sum_{t=1}^T \mathbb{E}[\|\nabla f(W_t)\|_{1,2}] \leq \frac{\Delta}{\eta} + 2 \sum_{t=1}^T \mathbb{E}[\|E_t\|_{1,2}] + \frac{TL_F\eta m}{2}.$$

We now apply Lemma A.10 to bound the error accumulation:

$$\sum_{t=1}^T \mathbb{E}[\|E_t\|_{1,2}] \leq (T-1) \frac{L_F\eta m\beta}{1-\beta} + T \frac{\sqrt{m}\sigma}{\sqrt{B}} \sqrt{\frac{1-\beta}{1+\beta}}.$$

Substituting this bound:

$$\begin{aligned} \sum_{t=1}^T \mathbb{E}[\|\nabla f(W_t)\|_{1,2}] &\leq \frac{\Delta}{\eta} + 2 \left[ (T-1) \frac{L_F\eta m\beta}{1-\beta} + T \frac{\sqrt{m}\sigma}{\sqrt{B}} \sqrt{\frac{1-\beta}{1+\beta}} \right] \\ &\quad + \frac{TL_F\eta m}{2}. \end{aligned}$$

Dividing both sides by  $T$ :

$$\begin{aligned} \frac{1}{T} \sum_{t=1}^T \mathbb{E}[\|\nabla f(W_t)\|_{1,2}] &\leq \frac{\Delta}{T\eta} + 2 \left[ \frac{T-1}{T} \cdot \frac{L_F\eta m\beta}{1-\beta} \right. \\ &\quad \left. + \frac{\sqrt{m}\sigma}{\sqrt{B}} \sqrt{\frac{1-\beta}{1+\beta}} \right] + \frac{L_F\eta m}{2}. \end{aligned}$$

Since  $\frac{T-1}{T} = 1 - \frac{1}{T}$ , we obtain:

$$\begin{aligned} \frac{1}{T} \sum_{t=1}^T \mathbb{E}[\|\nabla f(W_t)\|_{1,2}] &\leq \frac{\Delta}{T\eta} + 2 \left[ \left(1 - \frac{1}{T}\right) \frac{L_F\eta m\beta}{1-\beta} \right. \\ &\quad \left. + \frac{\sqrt{m}\sigma}{\sqrt{B}} \sqrt{\frac{1-\beta}{1+\beta}} \right] + \frac{L_F\eta m}{2}. \end{aligned}$$

This completes the proof.  $\square$

## B Analysis of MUON Preconditioner

This section provides implementation details for the diagonal dominance analysis presented in Section 3.2.

**Metric Computation** For each matrix parameter  $V_t \in \mathbb{R}^{m \times n}$  in the network, we compute the diagonal dominance metrics as follows:

1. **Gram Matrix Computation:** We first compute the Gram matrix  $G = V_t V_t^T \in \mathbb{R}^{m \times m}$ .
2. **Row-wise Ratio Calculation:** For each row  $i \in \{1, \dots, m\}$ , we compute the ratio  $r_i$  between the diagonal element and the average magnitude of off-diagonal elements:

$$r_i = \frac{G_{ii}}{\frac{1}{m-1} \sum_{j \neq i} |G_{ij}|} \quad (10)$$

where  $G_{ii} = \|V_{t,i}\|_2^2$  is the squared norm of the  $i$ -th row of  $V_t$ .

3. **Per-Parameter Aggregation:** For each matrix parameter, we aggregate the row-wise ratios into three statistics:

$$r_{\text{avg}} = \frac{1}{m} \sum_{i=1}^m r_i, \quad (11)$$

$$r_{\text{min}} = \min_{i \in \{1, \dots, m\}} r_i, \quad (12)$$

$$r_{\text{max}} = \max_{i \in \{1, \dots, m\}} r_i. \quad (13)$$

4. **Global Aggregation:** The global statistics  $\bar{r}_{\text{avg}}$ ,  $\bar{r}_{\text{min}}$ , and  $\bar{r}_{\text{max}}$  are computed by averaging the corresponding per-parameter metrics across all  $K$  matrix parameters in the network:

$$\bar{r}_{\text{avg}} = \frac{1}{K} \sum_{k=1}^K r_{\text{avg}}^{(k)}, \quad (14)$$

$$\bar{r}_{\text{min}} = \frac{1}{K} \sum_{k=1}^K r_{\text{min}}^{(k)}, \quad (15)$$

$$\bar{r}_{\text{max}} = \frac{1}{K} \sum_{k=1}^K r_{\text{max}}^{(k)}, \quad (16)$$

where the superscript  $(k)$  denotes the metric for the  $k$ -th matrix parameter.

**Logging Configuration** We use Weights & Biases (wandb) for metric tracking. The diagonal dominance ratios are computed and logged at every training step. The metrics are computed within the optimizer’s `step()` function, immediately after the momentum update and before the Newton-Schulz orthogonalization. In distributed training settings, the per-parameter metrics are computed locally on each GPU (parameters are distributed across GPUs), and the global statistics are synchronized via `all_reduce` operations.

**Model and Training Configuration** We conduct the analysis on both GPT-2 and LLaMA model families to align with the main pre-training setting. For GPT-2, we analyze Small (125M), Medium (355M), and Large (770M) on OpenWebText; for LLaMA, we analyze 60M, 130M, and 350M on C4. Model scales, training steps, warm-up schedules, sequence length, and batch size follow the settings in Section D.2 (Appendix D.2). In particular, GPT-2 uses 10K/20K/40K steps with sequence length 1024 and batch size 480, while LLaMA uses 10K/20K/60K steps with sequence length 256 and batch size 512. Optimization hyperparameters follow Appendix D.1; specifically, we use MUON with momentum 0.95, weight decay 0.1, and Newton-Schulz iteration steps of 5.

**Visualization** In Figures 7 and 8, the transparent curves represent the raw logged values, while the solid curves are smoothed using simple moving average with a window size of 50. The red dashed line at  $y = 1$  serves as a reference threshold—values above this line indicate that the diagonal elements dominate over the average off-diagonal magnitude, confirming diagonal dominance of the Gram matrix. The corresponding LLaMA results are shown in Figures 9 and 10.

## C Preconditioning Process Wall-Clock Time

This section provides detailed efficiency measurements for the preconditioning time cost analysis presented in Section 4.2. As shown in Table 3, RMNP achieves significant speedups over MUON across all model sizes while maintaining identical memory usage. Specifically, RMNP reduces the preconditioner computation time by approximately  $13\times$  to  $43\times$ , demonstrating its scalability advantage for large-scale training.

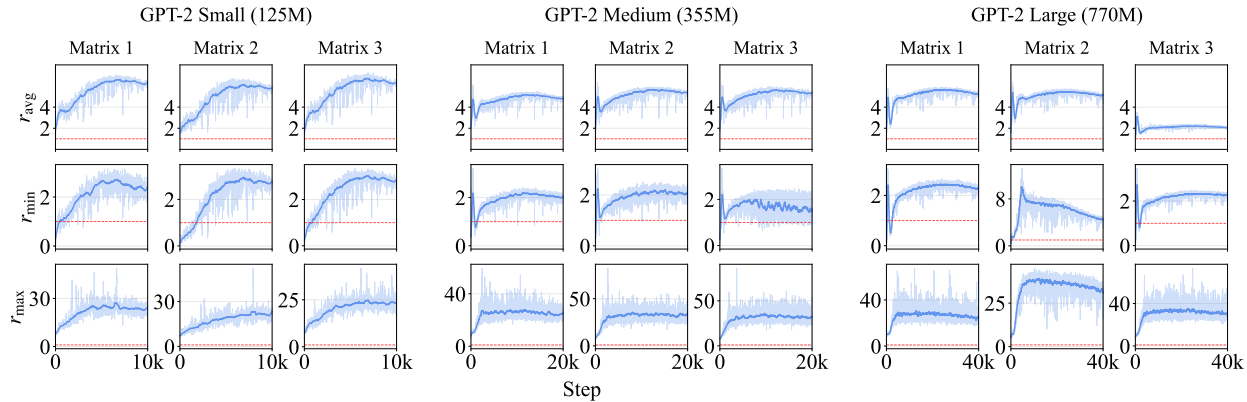


Figure 7: Per-parameter diagonal dominance ratios  $r_{\text{avg}}$ ,  $r_{\text{min}}$ ,  $r_{\text{max}}$  (rows) for three representative matrix parameters (columns) during GPT-2 Small (125M), GPT-2 Medium (355M), and GPT-2 Large (770M) pre-training. Transparent curves: raw values; solid curves: smoothed with window size 50. Red dashed line:  $y = 1$  threshold.

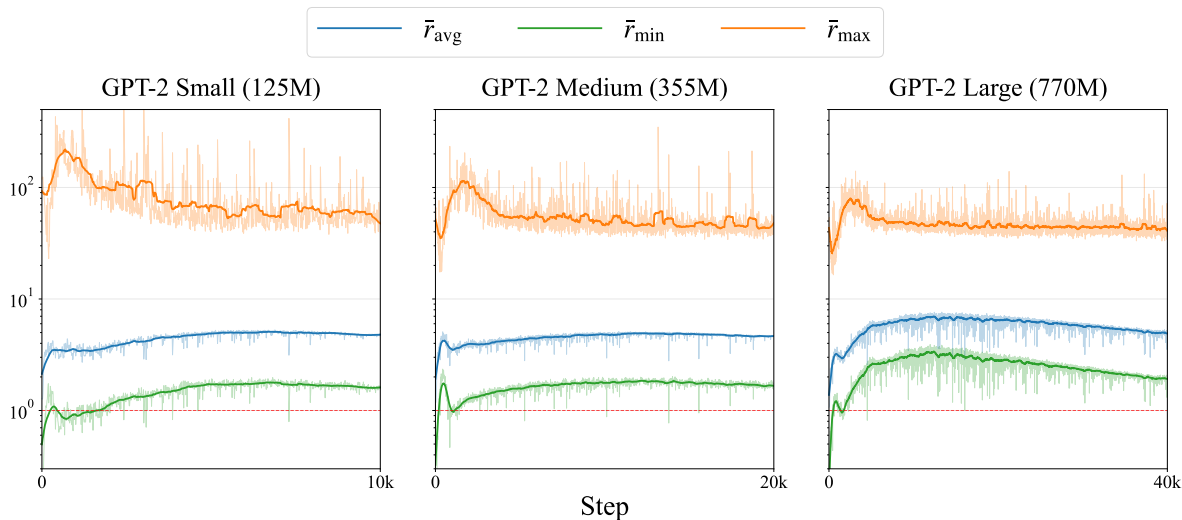


Figure 8: Global diagonal dominance ratios  $\bar{r}_{\text{avg}}$ ,  $\bar{r}_{\text{min}}$ ,  $\bar{r}_{\text{max}}$  averaged across all matrix parameters during GPT-2 Small (125M), GPT-2 Medium (355M), and GPT-2 Large (770M) pre-training. Y-axis in log scale. Transparent curves: raw values; solid curves: smoothed with window size 50. Red dashed line:  $y = 1$  threshold.

## C.1 Model Configuration for Preconditioning Time Cost

Table 4 presents the detailed model configurations used for measuring preconditioning time cost in Section 4.2.

## D Hyperparameter Search for Pretraining Performance

This section provides detailed hyperparameter search results for the pretraining experiments described in Section 4.3. We perform a systematic hyperparameter grid search for both RMNP and MUON across GPT-2 (Small and Medium) and LLaMA (60M, 130M, and 350M) models. Following the standard MUON training protocol, RMNP is integrated with ADAMW, with the learning rate decoupled into  $\text{lr}_{\text{AdamW}}$  and  $\text{lr}_{\text{Matrix}}$ . We

Table 3: Efficiency comparison between MUON (Newton-Schulz orthogonalization) and RMNP (row normalization) on GPT-2 models. Time and memory usage are measured over 100 steps with batch size 16 on one single RTX Pro 6000 GPU.

Size	Time Cost (s)		Memory (MB)	
	MUON	RMNP	MUON	RMNP
60M	1.480	<b>0.115</b>	7804	7804
125M	2.975	<b>0.201</b>	11797	11797
200M	4.140	<b>0.260</b>	15352	15352
355M	7.380	<b>0.401</b>	23225	23225
500M	15.720	<b>0.462</b>	30011	30011
770M	27.070	<b>0.611</b>	41508	41508
1.3B	30.570	<b>0.783</b>	61043	61043
1.5B	36.650	<b>0.855</b>	69465	69465

Table 4: GPT-2 Model Configurations for Preconditioning Time Cost

Model	Params	Layers	Heads	$d_{\text{model}}$
GPT-2 60M	60M	6	10	640
GPT-2 Small	125M	12	12	768
GPT-2 200M	200M	16	14	896
GPT-2 Medium	355M	24	16	1024
GPT-2 500M	500M	28	18	1152
GPT-2 Large	770M	36	20	1280
GPT-2 1.3B	1.3B	44	24	1536
GPT-2 XL	1.5B	48	25	1600

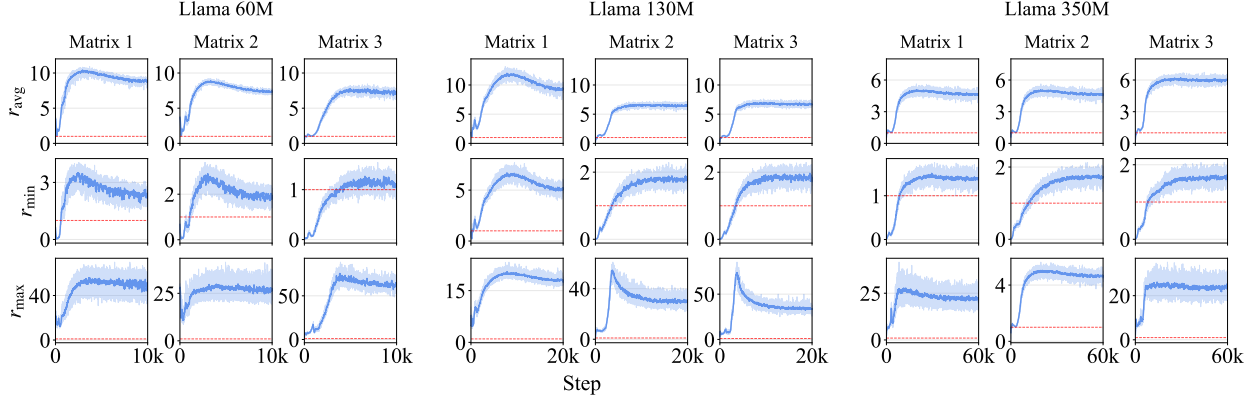


Figure 9: Per-parameter diagonal dominance ratios  $r_{\text{avg}}$ ,  $r_{\text{min}}$ ,  $r_{\text{max}}$  (rows) for three representative matrix parameters (columns) during LLaMA 60M, LLaMA 130M, and LLaMA 350M pre-training. Transparent curves: raw values; solid curves: smoothed with window size 50. Red dashed line:  $y = 1$  threshold.

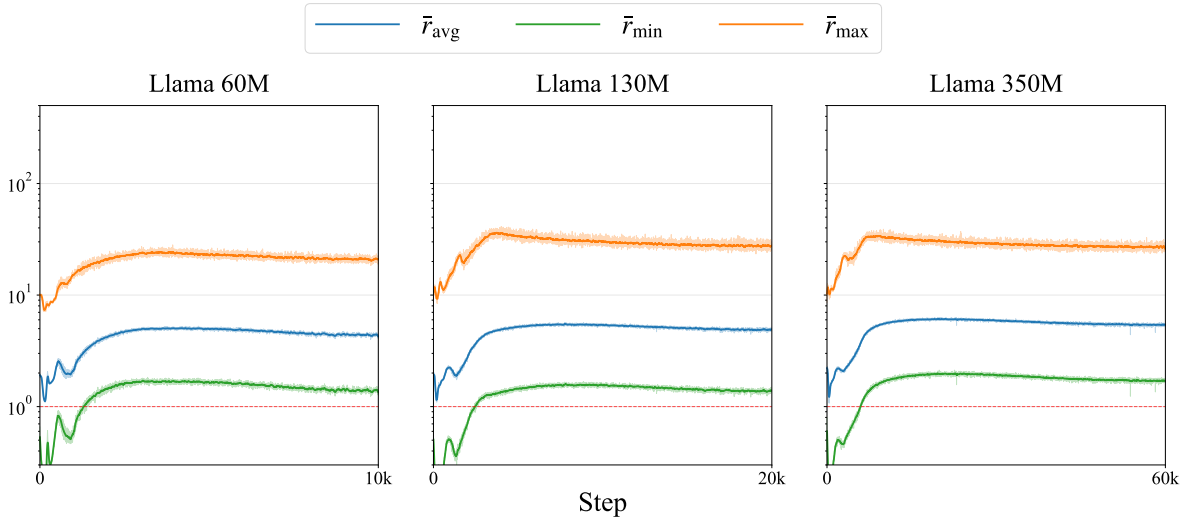


Figure 10: Global diagonal dominance ratios  $\bar{r}_{\text{avg}}$ ,  $\bar{r}_{\text{min}}$ ,  $\bar{r}_{\text{max}}$  averaged across all matrix parameters during LLaMA 60M, LLaMA 130M, and LLaMA 350M pre-training. Y-axis in log scale. Transparent curves: raw values; solid curves: smoothed with window size 50. Red dashed line:  $y = 1$  threshold.

fix  $\text{lr}_{\text{AdamW}}$  and vary  $\text{lr}_{\text{Matrix}}$  to evaluate its impact on convergence. The results are summarized in Tables 10 and 11 for GPT-2, and Tables 12, 13, and 14 for LLaMA. All values reported are evaluation perplexity (lower is better). We also present GPT-2 experiments on FineWeb-Edu-100B [41]; see Tables 6, 7, and 8 in Appendix D.2.

## D.1 Hyperparameter Settings

This section provides detailed hyperparameter settings for the experiments described in Section 4.1.

**MUON** For MUON, we set the momentum to 0.95 and weight decay to 0.1. Following Jordan et al. [11], we apply an RMS scaling coefficient to the learning rate:

$$\eta = \text{lr}_{\text{Matrix}} \cdot \max\left(1, \sqrt{\frac{n}{m}}\right), \quad (17)$$

where  $m$  and  $n$  denote the number of rows and columns of the parameter matrix, respectively. During hyperparameter search, we exclusively tune  $\text{lr}_{\text{Matrix}}$ . For ADAMW, we set  $\text{lr}_{\text{AdamW}} = 0.003, 0.0015, \text{ and } 0.001$  for GPT-2 Small, medium, and large models, respectively.

**RMNP** To ensure a fair comparison, we adopt the same RMS scaling as MUON:

$$\eta = \text{lr}_{\text{Matrix}} \cdot \max\left(1, \sqrt{\frac{n}{m}}\right), \quad (18)$$

as well as identical hyperparameters for ADAMW.

## D.2 Model Configurations

In this section, we present the model configurations and hyperparameters for GPT-2 (Table 5), GPT-2 on FineWeb-Edu-100B (Table 6), and LLaMA (Table 9). All GPT-2 models are trained with a maximum sequence length of 1024 and a batch size of 480. All LLaMA models are trained with a maximum sequence length of 256 and a batch size of 512. GPT-2 Small and medium models are trained in parallel on 4 NVIDIA RTX Pro 6000 GPUs, while GPT-2 large models are trained on a single NVIDIA Blackwell B200 Tensor Core GPU. LLaMA-60M and LLaMA-130M are trained in parallel on 2 NVIDIA L40. LLaMA-350M is trained in parallel on 4 NVIDIA RTX Pro 6000. For FineWeb-Edu-100B [41]<sup>1</sup>, the GPT-2 Small, Medium, and Large configurations are identical to the OpenWebText setup. Optimizer hyperparameters are listed in Table 7, and evaluation results in Figure 11 and Table 8.

Table 5: GPT-2 Model Configurations and specified hyperparameters

Model	Params	Layer	Heads	$d_{\text{emb}}$	Steps	Warm-up	Token Count	Batch Size	LR schedule
GPT-2 Small	125M	12	12	768	10K	1K	5B	480	Cosine
GPT-2 Medium	355M	24	16	1024	20K	2K	10B	480	Cosine
GPT-2 Large	770M	36	20	1280	40K	4K	20B	480	Cosine

Table 6: GPT-2 Model Configurations and specified hyperparameters for FineWeb-Edu-100B experiments.

Model	Params	Layer	Heads	$d_{\text{emb}}$	Steps	Warm-up	Token Count	Batch Size	LR schedule
GPT-2 Small	125M	12	12	768	10K	1K	5B	480	Cosine
GPT-2 Medium	355M	24	16	1024	20K	2K	10B	480	Cosine
GPT-2 Large	770M	36	20	1280	40K	4K	20B	480	Cosine

<sup>1</sup>We use the shuffled version by Karpathy [45]: <https://huggingface.co/datasets/karpathy/fineweb-edu-100b-shuffle>.

Table 7: Optimizer hyperparameters for GPT-2 pre-training on FineWeb-Edu-100B.

Model	Optimizer	$lr_{\text{AdamW}}$	$lr_{\text{Matrix}}$	Weight Decay	$\beta$	Schedule
Small (125M)	ADAMW	$6 \times 10^{-4}$	—	0.1	(0.9, 0.95)	Cosine
	MUON	$3 \times 10^{-3}$	$2 \times 10^{-2}$	0.1	(0.9, 0.95)	Cosine
	RMNP	$3 \times 10^{-3}$	$2 \times 10^{-2}$	0.1	(0.9, 0.95)	Cosine
Medium (355M)	ADAMW	$3 \times 10^{-4}$	—	0.1	(0.9, 0.95)	Cosine
	MUON	$1.5 \times 10^{-3}$	$1 \times 10^{-2}$	0.1	(0.9, 0.95)	Cosine
	RMNP	$1.5 \times 10^{-3}$	$1 \times 10^{-2}$	0.1	(0.9, 0.95)	Cosine
Large (770M)	ADAMW	$2 \times 10^{-4}$	—	0.1	(0.9, 0.95)	Cosine
	MUON	$1 \times 10^{-3}$	$6.67 \times 10^{-3}$	0.1	(0.9, 0.95)	Cosine
	RMNP	$1 \times 10^{-3}$	$6.67 \times 10^{-3}$	0.1	(0.9, 0.95)	Cosine

Table 8: Evaluation perplexity on FineWeb-Edu-100B for GPT-2 models. Small trained with 5B tokens; Medium with 10B tokens; Large with 20B tokens. Lower is better.

	Small (125M)	Medium (355M)	Large (770M)
ADAMW	23.85	18.19	14.81
MUON	22.71	17.13	14.16
RMNP	<b>22.60</b>	<b>17.07</b>	<b>13.75</b>

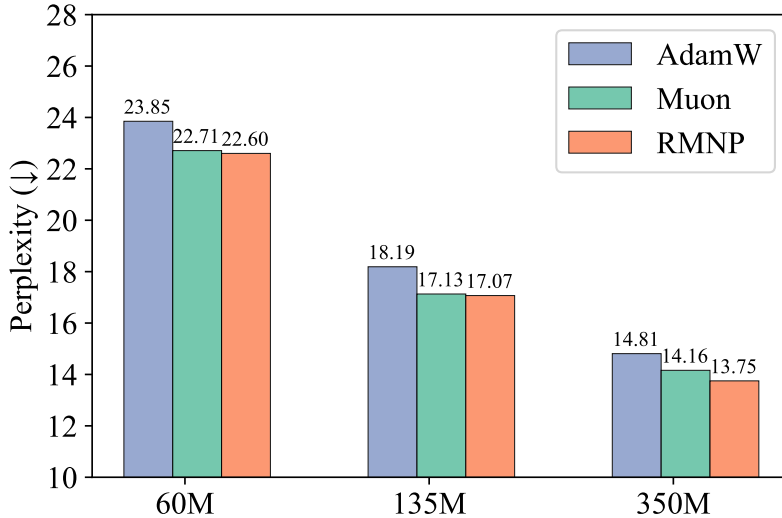


Figure 11: Results for GPT-2 on FineWeb-Edu-100B: Small (125M) trained with 5B tokens; Medium (355M) trained with 10B tokens, and Large (770M) trained with 20B tokens.

Table 9: LLaMA Model Configurations and specified hyperparameters.

Params	Hidden	Intermediate	Heads	Blocks	Steps	Warm-up	Token Count	Batch Size	LR schedule
60M	512	1376	8	8	10K	1K	1B	512	Cosine
130M	768	2048	12	12	20K	2K	2B	512	Cosine
350M	1024	2736	16	24	60K	6K	6B	512	Cosine

Table 10: Hyperparameter search on GPT-2 Small with ADAMW learning rate fixed at  $3 \times 10^{-3}$ .

Matrix LR	0.01	0.015	0.02	0.025
MUON	23.62	26.74	<b>22.86</b>	22.87
Matrix LR	0.002	0.003	0.004	0.005
RMNP	23.58	22.95	<b>22.82</b>	26.42

Table 11: Hyperparameter search on GPT-2 Medium with ADAMW learning rate fixed at  $1.5 \times 10^{-3}$ .

Matrix LR	0.005	0.01	0.02	0.03
MUON	18.33	18.26	<b>17.38</b>	17.44
Matrix LR	0.001	0.002	0.003	0.005
RMNP	18.58	<b>17.31</b>	17.42	17.88

Table 12: Hyperparameter search on LLaMA-60M. Validation perplexity is reported.

Matrix LR	0.005	0.01	0.02	0.03	0.04
MUON	29.90	<b>29.58</b>	30.46	30.49	30.03
Matrix LR	0.001	0.004	0.005	0.01	0.02
RMNP	31.00	28.99	<b>28.95</b>	29.26	29.64

Table 13: Hyperparameter search on LLaMA-130M. Validation perplexity is reported.

Matrix LR	0.005	0.01	0.02	0.03
MUON	22.51	<b>22.42</b>	22.47	22.51
Matrix LR	0.01	0.02	0.03	0.04
RMNP	22.42	22.49	<b>22.14</b>	23.31

Table 14: Hyperparameter search on LLaMA-350M. Validation perplexity is reported.

Matrix LR	0.003	0.004	0.005
MUON	17.01	<b>16.87</b>	16.89
Matrix LR	0.003	0.004	0.005
RMNP	17.02	16.86	<b>16.85</b>